Journal of Quantitative Spectroscopy & Radiative Transfer 204 (2018) 42–55

Contents lists available at ScienceDirect

Journal of Quantitative Spectroscopy & Radiative Transfer

journal homepage: www.elsevier.com/locate/jqsrt

MARVEL analysis of the measured high-resolution rovibrational spectra of C_2H_2

Katy L. Chubb[a,*], Megan Joseph[b], Jack Franklin[b], Naail Choudhury[b], Tibor Furtenbacher[c], Attila G. Császár[c], Glenda Gaspard[b], Patari Oguoko[b], Adam Kelly[b], Sergei N. Yurchenko[a], Jonathan Tennyson[a,*], Clara Sousa-Silva[d,a,b]

[a] Department of Physics and Astronomy, University College London, London WC1E 6BT, UK
[b] Highams Park School, Handsworth Avenue, Highams Park, London E4 9PJ, UK
[c] Institute of Chemistry, Eötvös Loránd University and MTA-ELTE Complex Chemical Systems Research Group, H-1518 Budapest 112, Hungary
[d] Department of Earth, Atmospheric and Planetary Sciences, Massachusetts Institute of Technology, 77 Massachusetts Ave, Cambridge, MA 02139, USA

ARTICLE INFO

Article history:
Received 19 July 2017
Revised 23 August 2017
Accepted 23 August 2017
Available online 24 August 2017

ABSTRACT

Rotation-vibration energy levels are determined for the electronic ground state of the acetylene molecule, $^{12}C_2H_2$, using the Measured Active Rotational-Vibrational Energy Levels (MARVEL) technique. 37,813 measured transitions from 61 publications are considered. The distinct components of the spectroscopic network linking *ortho* and *para* states of the molecule are considered separately. The 20,717 *ortho* and 17,096 *para* transitions measured experimentally are used to determine 6013 *ortho* and 5200 *para* energy levels. The MARVEL results are compared with alternative compilations based on the use of effective Hamiltonians.

1. Introduction

Acetylene, HCCH, is a linear tetratomic unsaturated hydrocarbon whose rovibronic spectrum is important in a large range of environments. The temperatures of these environments range from the hot, oxy-acetyene flames which are widely used for welding and related activities [1], temperate, where monitoring of acetylene in breath gives insights into the nature of exhaled smoke [2], to the cold, where the role of acetylene in the formation of carbon dust in the interstellar medium is a subject of debate [3]. Furthermore, acetylene is observed in star-forming regions [4] and thought to be an important constituent of clouds in the upper atmospheres of brown dwarfs and exoplanets [5]. Acetylene provides a major source of opacity in the atmospheres of cool carbon stars [6,7]. It is present in various planetary and lunar atmospheres in the solar system, including Jupiter and Titan [8], and has been detected on comets [9]. The first analysis of the atmosphere of a super-Earth exoplanet, 55 Cancri e [10], speculate that acetylene could be present in its atmosphere; however, the spectral data currently available does not allow for an accurate verification of the presence of acetylene in such a high-temperature environment.

The high-resolution spectrum of acetylene has long been studied in the laboratory, particularly by the group of Herman in Brussels. A full analysis of these experimental studies is given below. Herman and co-workers have written a number of reviews about the rovibrational behaviour of acetylene in its $\tilde{X}\,^1\Sigma_g^+$ ground electronic state [11–13]. Besides summarizing the status of the rotation-vibration spectroscopy of the system, these reviews also give insight into the internal dynamics of the system, a topic not considered here.

A number of variational nuclear motion calculations have been performed for the ground electronic state of acetylene [14–19]. New theoretical rovibrational calculations for this molecule are in progress as part of the ExoMol project [20,21], a database of theoretical line lists for molecules of astrophysical importance, appropriate up to high temperatures of around 3000 K, for use in characterising the atmospheres of cool stars and exoplanets. High accuracy experimental energy levels, like those obtained in this study, provide essential input for testing and improving theoretically calculated line positions.

In this work we present the largest compilation of published experimental rovibrational transitions for the $^{12}C_2H_2$ molecule, which has been formatted and analysed using the MARVEL (Measured Active Rotational-Vibrational Energy Levels) spectroscopic

* Corresponding authors.
E-mail addresses: katy.chubb.14@ucl.ac.uk (K.L. Chubb), j.tennyson@ucl.ac.uk (J. Tennyson).

http://dx.doi.org/10.1016/j.jqsrt.2017.08.018

Table 1
Quantum numbers used to label the upper and lower energy states of $^{12}C_2H_2$.

Label	Description
v_1	CH symmetric stretch (σ_g^+)
v_2	CC symmetric stretch (σ_g^+)
v_3	CH antisymmetric stretch (σ_u^+)
v_4	Symmetric (trans) bend (π_g)
ℓ_4	Vibrational angular momentum associated with v_4
v_5	Antisymmetric (cis) bend (π_u)
ℓ_5	Vibrational angular momentum associated with v_5
K	Total vibrational angular momentum, $\lvert\ell_4 + \ell_5\rvert$, and rotational quantum number
J	Rotational angular momentum
e/f	Symmetry relative to the Wang transformation (see text)
ortho/para	Nuclear spin state (see text)

Table 2
Parity of states in $^{12}C_2H_2$ based on the symmetry labels used in this work.

e/f	*J*	Parity
e	Odd	−
e	Even	+
f	Odd	+
f	Even	−

Table 3
Allowed combinations of symmetry labels for rovibrational states (including nuclear spin) of $^{12}C_2H_2$, where s = symmetric, a = antisymmetric, 'Total' is how the ro-vibronic wavefunction, including the nuclear spin, acts under permutation symmetry.

u/g	+/−	Ro-vib.	Nuclear spin	Total
u	+	*a*	*Ortho*	*a*
u	−	*s*	*Para*	*a*
g	+	*s*	*Para*	*a*
g	−	*a*	*Ortho*	*a*

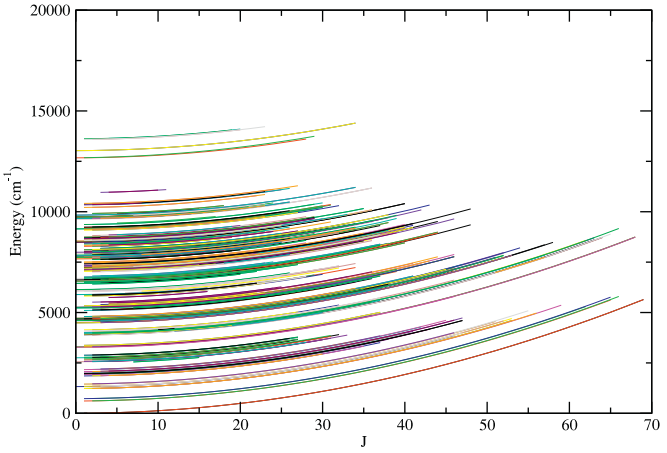

Fig. 1. MARVEL energy levels (cm^{-1}) as a function of rotational quantum number, *J*, for all the vibrational bands in the *ortho* network component analysed in this paper.

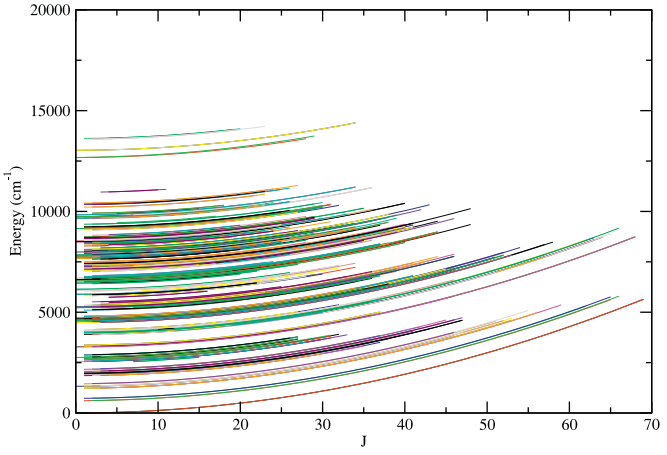

Fig. 2. MARVEL energy levels (cm^{-1}) as a function of rotational quantum number, *J*, for all the vibrational bands in the *para* network component analysed in this paper.

network software, the results of which are presented and discussed in this paper. The next section gives the underlying theory used for the study. Section 3 presents and discusses the experimental sources used. Results are given in Section 4. Section 5 discusses these results; this section presents comparisons with recent empirical databases due to Amyay et al. [22] (henceforth 16AmFaHe), Lyulin and Campargue [23] (henceforth 17LyCa) and Lyulin and Perevalov [24] (henceforth 17LyPe), which builds on their earlier work [25], all of which only became available while the present study was being undertaken. Finally, Section 6 gives our conclusions.

2. Theory

2.1. MARVEL

The MARVEL procedure [26,27] is based on the theory of spectroscopic networks (SNs) [28,29] and is principally based on earlier work by Flaud et al. [30] and Watson [31,32]. The MARVEL protocol can be used to critically evaluate and validate experimentally-determined transition wavenumbers and uncertainties collected from the literature. It inverts the wavenumber information to obtain accurate energy levels with an associated uncertainty. MARVEL has been successfully used to evaluate empirical energy levels for molecules such as TiO [33], $^{14}NH_3$ [34,35], water vapour [36–40], H_2D^+ and D_2H^+ [41], H_3^+ [42], and C_2 [43]. To be useful for MARVEL, measured transitions must have an associated uncertainty and each state must be uniquely labelled, typically by a set of quantum numbers. It should be noted that while MARVEL requires uniqueness it does not require these quantum numbers to be strictly correct, or indeed even meaningful, beyond obeying rigorous selection rules; these assignments simply act as labels for each state. Nevertheless, it greatly aids comparisons with other data if they contain physically sensible information. The quantum numbers used in the present study are considered in the following section.

2.2. Quantum number labelling

The 11 quantum numbers used in this study for labelling the upper and lower rovibrational states of $^{12}C_2H_2$ are detailed in Table 1. This label includes the quanta of excitation of each

Table 4
Extract from the MARVEL input file for the *ortho* transitions. The full file is supplied as part of the supplementary information to this paper. All energy term values and uncertainties are in units of cm^{-1}. The assignments are detailed in Table 1.

Energy	Uncertainty	Upper assignment	Lower assignment	Reference
1248.2620	0.0005	0 0 0 1 1 1 -1 0 34 e ortho	0 0 0 0 0 0 0 0 35 e ortho	00Vander_table2_l1
1252.8546	0.0005	0 0 0 1 1 1 -1 0 32 e ortho	0 0 0 0 0 0 0 0 33 e ortho	00Vander_table2_l2
1257.4230	0.0005	0 0 0 1 1 1 -1 0 30 e ortho	0 0 0 0 0 0 0 0 31 e ortho	00Vander_table2_l4
1261.9694	0.0005	0 0 0 1 1 1 -1 0 28 e ortho	0 0 0 0 0 0 0 0 29 e ortho	00Vander_table2_l6
1266.4970	0.0005	0 0 0 1 1 1 -1 0 26 e ortho	0 0 0 0 0 0 0 0 27 e ortho	00Vander_table2_l8
1271.0098	0.0005	0 0 0 1 1 1 -1 0 24 e ortho	0 0 0 0 0 0 0 0 25 e ortho	00Vander_table2_l10
1275.5122	0.0005	0 0 0 1 1 1 -1 0 22 e ortho	0 0 0 0 0 0 0 0 23 e ortho	00Vander_table2_l11

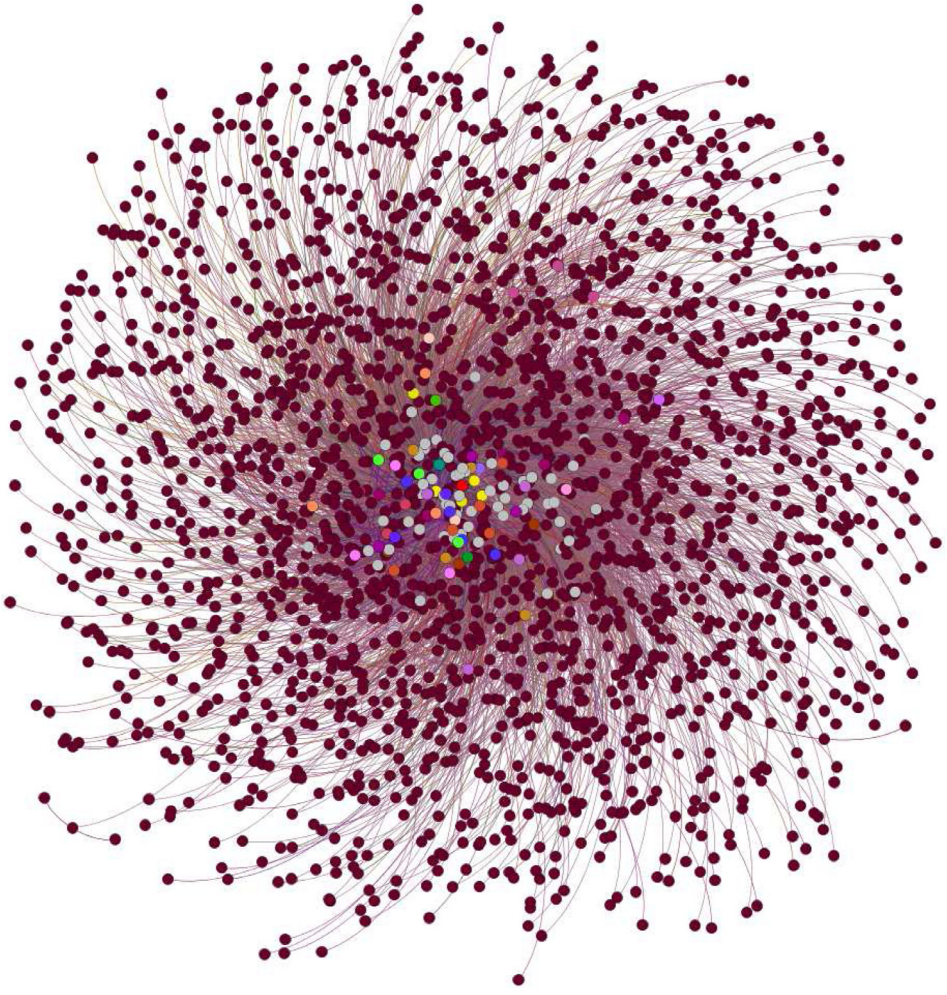

Fig. 3. *Ortho* component of the spectroscopic network of $^{12}C_2H_2$ produced using MARVEL input data.

vibrational mode in normal-mode notation: $v_1, v_2, v_3, v_4, \ell_4, v_5, \ell_5, K = |\ell_4 + \ell_5|$ and J, where $v_1, \ldots, v_5$ are the vibrational quantum numbers, ℓ_4 and ℓ_5 are the vibrational angular momentum quantum numbers associated with v_4 and v_5, respectively, with $|\ell| = v, v-2 \ldots 1$ for odd v, $|l| = v, v-2 \ldots 0$ for even v. $K = |k|$ is the rotational quantum number, with k corresponding to the projection of the rotational angular momentum, **J**, on the z axis. K is also equal to the total vibrational angular momentum quantum number, $|L| = |\ell_4 + \ell_5|$, and therefore K will be also referred to as the total vibrational angular momentum. J is the quantum number associated with rotational angular momentum, **J**. We follow the phase convention of the Belgium group [13] for $K \equiv |k| = |\ell_4 + \ell_5|$, with $\ell_4 \geq 0$ if $k = 0$. We also use the e or f labelling, along with the nuclear spin state (*ortho* or *para*).

The quantum number assignments for this work were taken from the original sources where possible, with any exceptions noted in Sections 3.1 and 3.2: particular reference should be made to the general comments (1) and (2) in 3.2. While MARVEL requires a unique set of quantum numbers for each state, it merely treats these as labels and whether they are strictly correct or not does not affect the validity of the results. Nevertheless, labelling with sensible assignments aids comparisons with other datasets.

Levels with parity $+(-1)^J$ are called e levels and those with parity $-(-1)^J$ are called f levels. In other words, e and f levels transform in the same way as the rotational levels of $^1\Sigma^+$ and $^1\Sigma^-$ states of linear molecules, respectively [44]. Table 2 gives the combinations of e/f and J with corresponding parity. States of a linear molecule are often also classified based on inversion, with states which are left unchanged

Table 5
Data sources used in this study with wavenumber range, numbers of transitions and approximate temperature of the experiment. A/V stands for the number of transitions analysed/verified. 'RT' stands for room temperature. See Section 3.1 for the notes.

Tag	Reference	Range (cm^{-1})	A/V	Bands	Temperature	Note
09YuDrPe	Yu et al. [51]	29–55	20/20	5	RT	
16AmFaHe_kab91	Kabbadj et al. [52]	61–1440	3233/3233	47	RT	
16AmFaHe_amy10	Amyay et al. [53]	63–7006	1232/1232	36	RT	
11DrYu	Drouin and Yu [54]	85–92	20/20	7	RT	
17JaLyPe	Jacquemart et al. [55]	429–592	627/627	9	RT	
81HiKa	Hietanen and Kauppinen [56]	628–832	684/684	5	RT	(3a)
93WeBlNa	Weber et al. [57]	632–819	1610/1609	13	RT	(3b)
00MaDaCl	Mandin et al. [58]	644–820	77/77	1	RT	
01JaClMa	Jacquemart et al. [59]	656–800	355/355	4	RT	
50BeNi	Bell and Nielsen [60]	671–4160	500/0	13	RT	(3c)
16AmFaHe_gom10	Gomez et al. [61]	1153–1420	27/27	3	RT	
16AmFaHe_gom09	Gomez et al. [62]	1247–1451	66/66	8	RT	
00Vander	Auwera [63]	1248–1415	64/64	2	RT	
16AmFaHe_amy09	Amyay et al. [64]	1253–3422	3791/3777	57	Up to 1455 K	(3d)
03JaMaDa	Jacquemart et al.[65]	1810–2235	486/486	14	RT	
03JaMaDab	Jacquemart et al. [66]	3207–3358	109/109	2	RT	
16AmFaHe_jac02	Jacquemart et al. [67]	1860–2255	150/150	3	RT	
72Pliva	Plíva [45]	1865–2598	1016/1015	15	RT	
16AmFaHe_ber98	Bermejo et al. [68]	1957–1960	19/19	1	RT	(3e)
16AmFaHe_jac07	Jacquemart et al. [69]	2515–2752	148/148	3	RT	
16AmFaHe_pal72	Palmer et al. [70]	2557–5313	42/42	3	RT	
16AmFaHe_vda93	Auwera et al. [71]	2584–3364	499/499	5	RT	
93DcSaJo	Dcunha et al. [72]	2589–2760	372/372	3	RT	
82RiBaRa	Rinsland et al. [6]	3140–3399	1789/1788	21	RT and 433 K	
16AmFaHe_sarb95	Sarma et al. [73]	3171–3541	401/401	8	RT	
06LyPeMa	Lyulin et al. [74]	3182–3327	167/167	13	RT	
16AmFaHe_man05	Mandin et al. [75]	3185–3355	288/288	5	RT	
16AmFaHe_sara95	Sarma et al. [76]	3230–3952	424/424	5	RT	
16AmFaHe_ber99	Bermejo et al. [77]	3358–3361	21/21	1	RT	(3e)
16AmFaHe_lyub07	Lyulin et al. [78]	3768–4208	668/668	8	RT	
16AmFaHe_gir06	Girard et al. [79]	3931–4009	91/91	10	RT	
16AmFaHe_dcu91	Dcuhna et al. [80]	3999–4143	251/251	6	RT	
72BaGhNa	Baldacci et al. [81]	4423–4791	472/408	8	RT	(3f)
16AmFaHe_lyua07	Lyulin et al. [82]	4423–4786	440/440	8	RT	
16AmFaHe_lyu08	Lyulin et al. [83]	5051–5562	320/320	7	RT	
16AmFaHe_kep96	Keppler et al. [84]	5705–6862	1957/1957	30	RT	
17LyCa	Lyulin and Campargue [23]	5852–8563	4941/4941	108	RT	(3g)
16AmFaHe_rob08	Robert et al. [85]	5885–6992	568/568	20	RT	
07TrMaDa	Tran et al. [86]	6299–6854	546/546	13	RT	(3h)
16AmFaHe_lyu09	Lyulin et al. [87]	6300–6666	89/89	5	RT	
16KaNaVa	Karhu et al. [88]	6386–6541	19/19	2	RT	(3i)
16AmFaHe_kou94	Kou et al. [89]	6439–6629	73/73	1	RT	
15TwCiSe	Twagirayezu et al. [90]	6448–6564	135/135	2	RT	
02HaVa	Hachtouki and Auwera [91]	6448–6685	271/271	4	RT	
77BaGhNa	Baldacci et al. [92]	6460–6680	860/859	15	RT	(3j)
05EdBaMa	Edwards et al. [93]	6472–6579	41/41	1	RT	
13ZoGiBa	Zolot et al. [94]	6490–6609	37/37	1	RT	
00MoDuJa	Moss et al. [95]	6502–6596	36/36	1	RT	
96NaLaAw	Nakagawa et al. [96]	6502–6596	36/36	1	RT	
16AmFaHe_amy11	Amyay et al. [97]	6667–7868	2259/2256	79	RT	(3k)
15LyVaCa	Lyulin et al. [98]	7001–7499	2471/2471	29	RT	(3l)
09JaLaMa	Jacquemart et al. [99]	7043–7471	233/233	4	RT	
02VaElBr	Auwera et al. [100]	7062–9877	626/626	11	RT	(3m)
16LyVaCa	Lyulin et al. [101]	8283–8684	627/627	14	RT	(3n)
17BeLyHu	Béguier et al. [102]	8994–9414	432/432	11	RT	
89HeHuVe	Herman et al. [103]	9362–10413	657/657	14	RT	(3o)
93SaKa	Sakai and Katayama [104]	12428–12538	91/73	1	RT	(3p)
03HeKeHu	Herregodts et al. [105]	12582–12722	60/60	1	RT	
92SaKa	Sakai and Katayama [106]	12904–13082	216/212	3	RT	(3q)
94SaSeKa	Sakai et al. [107]	13629–13755	53/53	1	<RT (223K)	(3r)
Total		29–13755	37813/37206			

called 'gerade' and labelled with a subscript *g*, and those whose phase changes to opposite are called 'ungerade' and labelled *u*. The *ortho* and *para* labels are defined based on the permutation, *P*, of the identical hydrogen atoms. For the *para* states the corresponding rovibrational wavefunctions, $\Psi_{r\text{-}v}$, are symmetric, i.e. $P\Psi_{r-v} = (+1)\Psi_{r-v}$, while for the *ortho* states they are antisymmetric, $P\Psi_{r-v} = (-1)\Psi_{r-v}$. The allowed combinations of these labels are shown in Table 3 and explained in more detail below.

The *e*/*f* labelling which has been adopted in this work was originally introduced by Brown et al. [44] to eliminate issues relating to Plíva's *c*/*d* labelling [45] and the *s*/*a* labelling of Winnewisser and Winnewisser [46]. For more detailed information on the *e*/*f* parity doublets, see the section titled '*e*/*f* levels' of Herman et al. [47]. In summary, an interaction known as

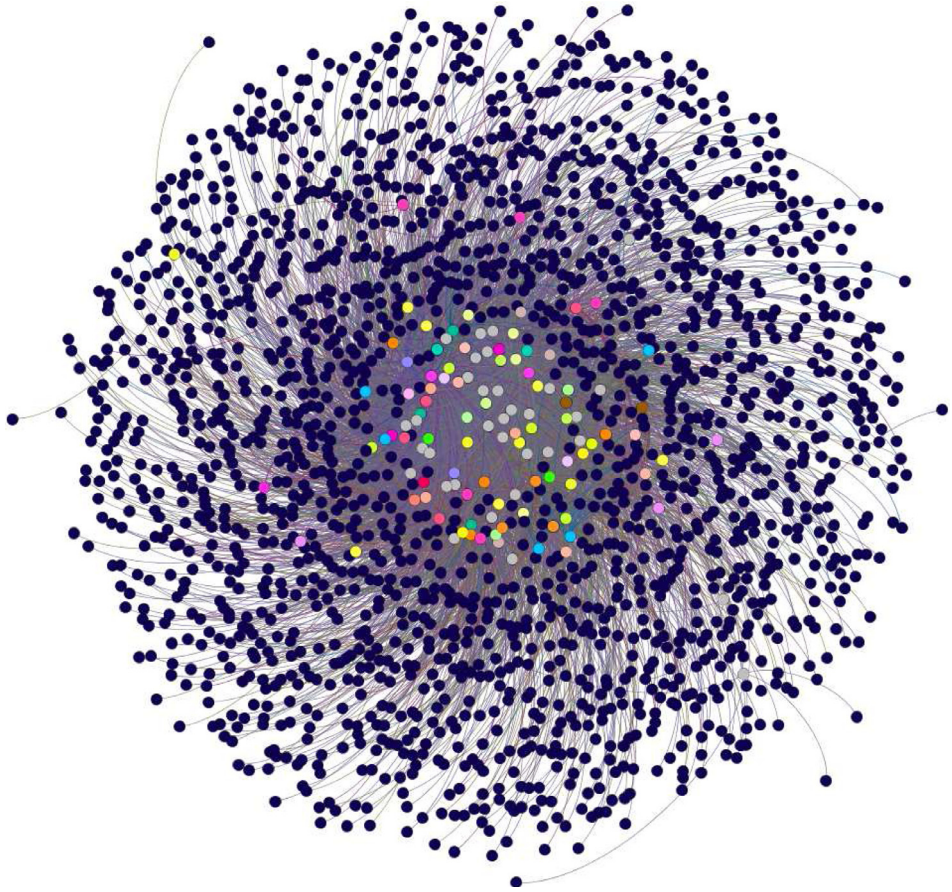

Fig. 4. *Para* component of the spectroscopic network of $^{12}C_2H_2$ produced using MARVEL input data.

ℓ-doubling occurs in linear molecules, which splits the rotational, J, levels in certain vibrational states. The symmetry describing these states is based on the total vibrational angular momentum quantum number, K. There are, for example, two distinct states in the $2\nu_4$ band; one with $K = 0$ (Σ_g^+, $(0002^00^0)^0$) and another with $K = 2$ (Δ_g, $(0002^20^0)^2$). In this case, the interaction with the rotation leads to a splitting of the rovibrational levels in the $K = 2$ (Δ_g) sublevel (ℓ-doubling). The Δ_e (corresponding to one of the two bending modes) and Σ_e (corresponding to one of the three stretching modes) states repel each other, pushing Δ_e to a lower energy while Δ_f is unaffected. For this reason the e state typically lies below the f state, as bending occurs at a lower frequency than stretching [47]. This effect depends on $J(J + 1)$ and so becomes increasingly important at higher rotational excitations. If a rovibrational state has no rotational splitting (as is the case if $\ell_4 = \ell_5 = 0$, but not if $\ell_4 = 1$ and $\ell_5 = -1$), the state is always labelled e and there is no corresponding f state.

Herman and Lievin [48] give an excellent description of the *ortho* and *para* states of acetylene; the treatment of the main isotopologue is summarised here. The hydrogen atoms are spin-$\frac{1}{2}$ particles and therefore obey Fermi-Dirac statistics. The ^{12}C atoms have zero nuclear spin and so do not need to be considered here. The symmetry operation, P, describes a permutation of identical particles; when applied to the $^{12}C_2H_2$ molecule it implies permutation of the two hydrogen atoms. For fermions the total wavefunction must be antisymmetric upon such a transformation. The permutation symmetry of the ground electronic state is totally symmetric upon interchange of identical atoms and so the electronic part of the wavefunction can be ignored here. The symmetry of the nuclear spin part of the wavefunction is not usually specified, but can easily be deduced from the remaining symmetry. If the rovibrational part of the wavefunction is antisymmetric under permutation symmetry (resulting from a combination of g and - or u and +), then the nuclear spin state must be *ortho*, and if the rovibrational part of the wavefunction is symmetric ($g, +$ or $u, -$), then the nuclear spin state must be *para* (see Table 3).

It is important to distinguish the vibrational and rotational symmetries from the symmetry of the rovibrational states of $\Psi_{\text{r-v}}$. For a linear molecule such as $^{12}C_2H_2$ both the rotational Ψ_{r} and the vibrational Ψ_{v} contributions to $\Psi_{\text{r-v}}$ should transform according with the point group $D_{\infty h}$ (M), spanning an infinite number of irreducible representations such as $\Sigma_{g/u}^{+/-}$ ($K = 0$), $\Pi_{g/u}^{+/-}$ ($K = 1$), $\Delta_{g/u}^{+/-}$ ($K = 2$) etc. However, after combining the rotational and vibrational parts into the rovibrational state $\Psi_{\text{r-v}}$, only the $K = 0$ states (i.e. Σ_g^+, Σ_g^-, Σ_u^+, Σ_u^-) can lead to the total nuclear-rotation-vibrational state obeying the proper statistics, as described above. These term symbols are the irreducible elements of the D_{2h}(M) group [49], which according to our labelling scheme correspond to the four pairs: *e ortho*, *e para*, *f ortho* and *f para*. For example, the vibrational state ν_5 (Π_u) can be combined with the $J = 1$, $K = 1$ (Π_g) rotational state to produce three rovibrational combinations of Σ_u^+, Σ_u^- and Π_u ($D_{\infty h}$ point group). However, only the Σ_u^-, Σ_u^+ states are allowed by nuclear-spin statistics. Here ν_5, Π_u, K, Π_g are not rigorous quantum numbers/labels, while $J = 1$, *e*/*f* and *ortho*/*para* are. Thus, these two rovibrational states are assigned $(0000^01^1)^1$, J= 1, *e*, *para* and $(0000^01^1)^1$, J=1, *f*, *ortho*, respectively. It should be also noted that generally neither K nor $\nu_1, \ldots, \nu_5$ are good quantum numbers. However, the quantity $(-1)^{\nu_3+\nu_5}$ is as it defines the conserved u/g symmetry as follows: a state is ungerade

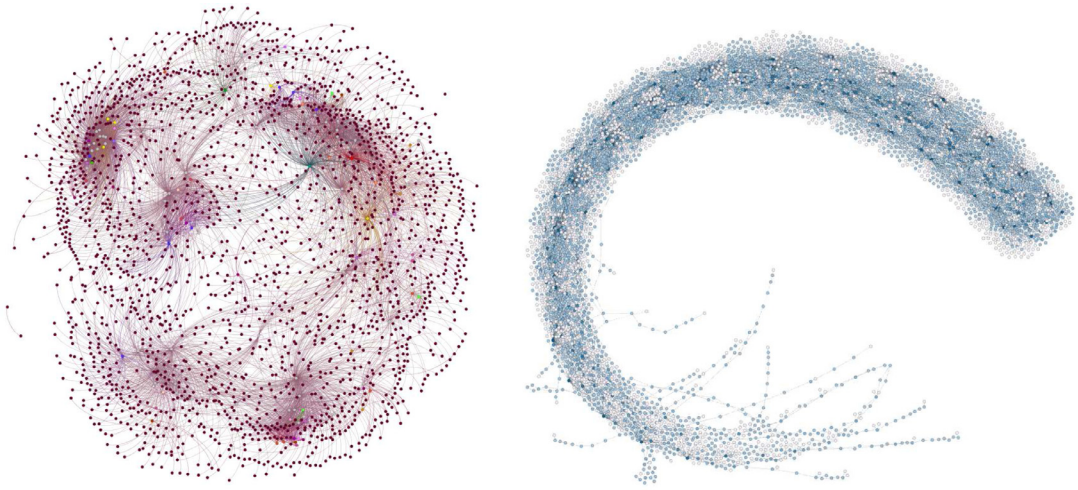

Fig. 5. Alternative representations of the *ortho* (left) and *para* (right) component of the spectroscopic networks of $^{12}C_2H_2$ produced using MARVEL input data.

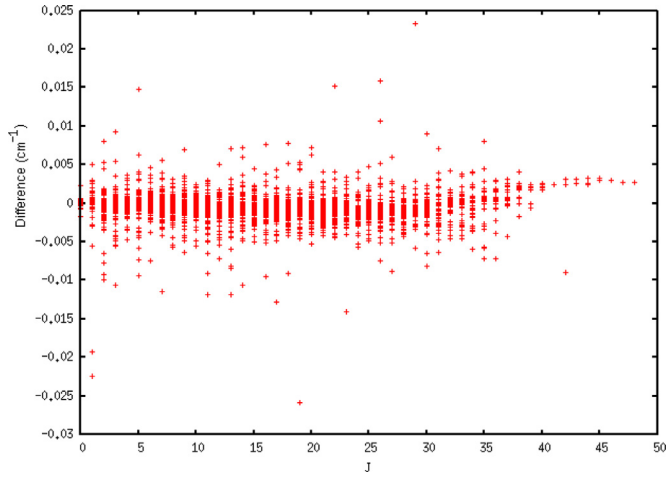

Fig. 6. Differences between the energy term values given in 17LyCa [23] and this work as a function of rotational angular momentum quantum number, *J*.

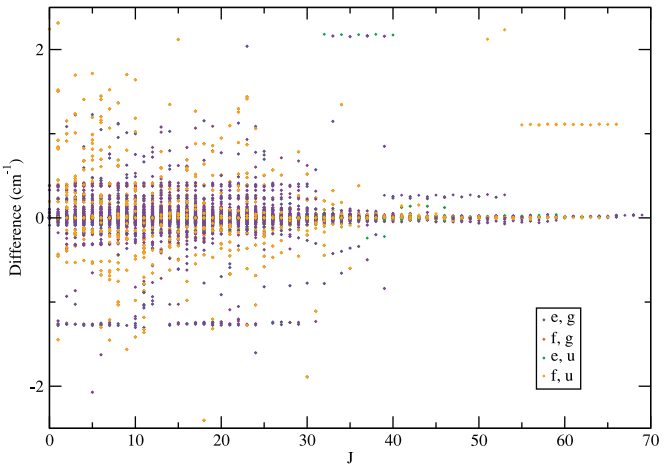

Fig. 7. Deviations, in cm^{-1}, between this work and 16AmFaHe [22] as a function of rotational angular momentum quantum number, *J*. Different colours represent different designations of *e*/*f* and *u*/*g*.

if $(-1)^{v_3+v_5} = -1$ and gerade if $(-1)^{v_3+v_5} = 1$. The +/− labelling is derived from *e*/*f* and *J*, as given in Table 2.

Throughout this paper we shall use the notations $(v_1v_2v_3v_4^{\ell_4}v_5^{\ell_5})^K$ to describe vibrational states and $(v_1v_2v_3v_4^{\ell_4}v_5^{\ell_5})^K$, *J*, *e*/*f*, *ortho*/*para* to describe rovibrational states. The *e* and *f* labelling combined with *J* and nuclear spin state (*ortho* or *para*) gives the rigorous designation of each state. Other quantum number labels are approximate but, besides representing the underlying physics, are necessary to uniquely distinguish each state. The symmetry labels of the vibrational states ($\Sigma^{+/-}_{u/g}$, $\Pi_{u/g}$, $\Delta_{u/g}$, ...) have been added to the end of the output energy files (see Table 8 and supplementary material).

2.3. Selection rules

The rigorous selection rules governing single-photon rotation-vibration transitions for a symmetric linear molecule (molecular symmetry (MS) group $D_{\infty h}$(M)) are given by

$$\Delta J = \pm 1 \quad \text{with} \quad e \leftrightarrow e \quad \text{or} \quad f \leftrightarrow f, \tag{1}$$

$$\Delta J = 0 \quad \text{with} \quad e \leftrightarrow f \tag{2}$$

$$J' + J'' \neq 0 \tag{3}$$

$$u \leftrightarrow g \tag{4}$$

The first two equations here correspond to the standard selection rule $+ \leftrightarrow -$ for the dipole transitions in terms of the parities. The *ortho* states of $^{12}C_2H_2$ have the statistical weight $g_{ns} = 3$, while for the *para* states $g_{ns} = 1$.

3. Experimental sources

A large number of experimentally-determined rovibrational transition frequencies can be found in the literature for the main isotopologue of acetylene, $^{12}C_2H_2$. As part of this study we attempted to conduct a rigorous and comprehensive search for all useable high-resolution spectroscopic data. This includes the transition frequency (in cm^{-1}) and associated uncertainty, along with quantum number assignments for both the upper and lower energy states. A unique reference label is assigned to each transition, which is required for MARVEL input. This label indicates the data source, table (or page) and line number that the transition originated from. The data source tag is based on the notation employed by an IUPAC Task Group on water spectroscopy

Table 6
Data sources considered but not used in this work.

Tag	Reference	Comments
16AmFaHe_abb96	Temsamani et al. [108]	0 transitions in 16AmFaHe; data not available in original paper.
16AmFaHe_eli98	Idrissi et al. [109]	0 transitions in 16AmFaHe; data not available in original paper.
72Plivaa	Plíva [110]:	Energy levels only
02MeYaVa	Metsälä et al. [111]	No suitable data
01MeYaVa	Metsälä et al. [112]	No suitable data
99SaPeHa	Saarinen et al. [113]	No suitable data
97JuHa	Jungner and Halonen [114]	No suitable data
93ZhHa	Zhan and Halonen [115]	No suitable data
93ZhVaHa	Zhan et al. [116]	No suitable data
91ZhVaKa	Zhan et al. [117]	No suitable data
13SiMeVa	Siltanen et al. [118]	No suitable data
83ScLeKl	Scherer et al. [119]	No assignments given

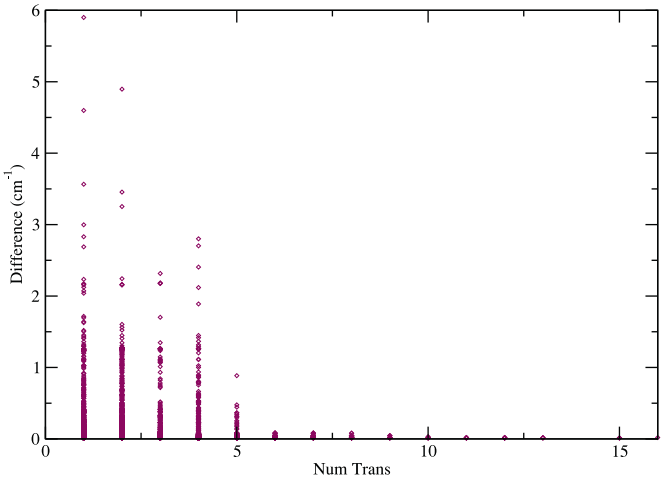

Fig. 8. Deviations, in cm^{-1}, between this work and 16AmFaHe [22] as a function of the number of transitions that link to the energy level in our dataset.

Table 7
Changes in labelling between 15LyVaCa [98], 17LyCa_FTS15 [23] and this work, in the form $(v_1v_2v_3v_4^{\ell_4}v_5^{\ell_5})^K$. See comment (3l) in the text.

15LyVaCa	17LyVa_FTS15	This work
$(0204^21^{-1})^{1**}$	$(0113^10^0)^1$	$(0204^11^0)^1$
$(0113^10^0)^1$	$(0204^01^1)^1$	$(0113^10^0)^1$
$(1102^01^1)^1$	$(1102^01^1)^1$	$(1102^11^0)^1$
$(1102^21^{-1})^{1**}$	$(0202^23^{-1})^1$	$(1102^01^1)^1$
$(1102^21^{-1})^{1*}$	$(1102^21^{-1})^1$	$(1102^21^{-1})^1$

[37,50] with an adjustment discussed below. The associated uncertainties were taken from the experimental data sources where possible, though it was necessary to increase many of these in order to achieve consistency with the same transition in alternative data sources. As noted by Lyulin and Perevalov [25], these sources often provide overall uncertainties for the strongest lines in a vibrational band which may underestimate the uncertainty associated with some or all of the weaker, and especially of blended, lines.

61 sources of experimental data were considered. Two of the data compilations mentioned in the introduction [22,23] contain data from multiple other sources, some of which was not directly available to us. Data taken from these compilations is given a tag based on that used in the compilation with the original reference given in Table 5. After processing, 60 sources were used in the final data set. The data from more recent papers is generally provided in digital format, but some of the older papers had to be processed through digitalisation software, or even manually entered in the most extreme cases. After digitalisation the data was converted to MARVEL format; an example of the input file in this format is given in Table 4; the full file can be found in the supplementary data of this paper.

Table 5 gives a summary of all the data sources used in this work, along with the wavenumber range, number of transitions, number of vibrational bands, the approximate temperature of the experiment, and comments, which can be found in Section 3.1. Table 6 gives those data sources which were considered but not used, with comments on the reasons. The reference label given in these tables corresponds to the unique labels in the MARVEL input files, given in the supplementary data and illustrated in the last column of Table 4. As transitions do not occur between *ortho* and *para* states, they form two completely separate components of the experimental spectroscopic network, with no links between them. All input and output files supplied in the supplementary data to this work are split into either *ortho* or *para*.

3.1. Comments on the experimental sources in Table 5

(3a) 81HiKa [56] has two apparent misprints: in column 2 of their Table 6, the R(19) line should be 780.2601 cm^{-1} and not 790.2601 cm^{-1}, as confirmed by 01JaClMa [59], and in column 5 of their Table 4 the Q(3) line should be 728.9148 cm^{-1} not 729.9148 cm^{-1}, also confirmed by 01JaClMa [59].

(3b) 93WeBlNa_page14_l38 from 93WeBlNa [57] is not consistent with other data sources. It was marked in the original dataset as a transition that the authors did not include in their analysis and so has been removed from our dataset.

(3c) 50BeNi [60] was deemed too unreliable to use in the final dataset: their data are directly contradicted by other sources.

(3d) Many of the transitions included from 16AmFaHe_amy09 [64] are not duplicated in any other source. While this means they represent a valuable source of data, and have thus been kept in the MARVEL dataset, the fact that there is no other experimental data to back them up means they should be treated with some degree of caution. As stated in the original paper, modelling such a high temperature region is a challenge. There are a small number of transitions - 14 out of 3791 - that do not match those from other data sources and have been removed from our final dataset.

(3e) 16AmFaHe_ber98 [68] and 16AmFaHe_ber99 [77] are Raman spectra and so the transitions do not follow the selection rules detailed in Section 2.3 of this paper.

(3f) 72BaGhNa [81] has a band labelled $(0013^10^0)^1$ - $(0001^10^0)^1$ which is not consistent with other data sources. It was found that the band labelled $(0104^01^1)^1$ - $(0001^10^0)^1$ gave energies consistent with those labelled $(0013^10^0)^1$ - $(0001^10^0)^1$

Table 8
Extract from the MARVEL output file for the *ortho* transitions. The full file is supplied as part of the supplementary information to this paper. All energies and uncertainties are in units of cm^{-1}. The assignments are detailed in Table 1.

Assignment											Energy	Uncertainty	NumTrans	u/g	Symmetry
0	0	0	0	0	0	0	0	1	e	ortho	2.35329	0.00003	204	g	sigma_g_plus
0	0	0	0	0	0	0	0	3	e	ortho	14.11952	0.00002	289	g	sigma_g_plus
0	0	0	0	0	0	0	0	5	e	ortho	35.29793	0.00002	306	g	sigma_g_plus
0	0	0	0	0	0	0	0	7	e	ortho	65.88710	0.00002	298	g	sigma_g_plus
0	0	0	0	0	0	0	0	9	e	ortho	105.88501	0.00002	306	g	sigma_g_plus
0	0	0	0	0	0	0	0	11	e	ortho	155.28899	0.00002	306	g	sigma_g_plus
0	0	0	0	0	0	0	0	13	e	ortho	214.09576	0.00002	306	g	sigma_g_plus
0	0	0	0	0	0	0	0	15	e	ortho	282.30144	0.00002	310	g	sigma_g_plus
0	0	0	0	0	0	0	0	17	e	ortho	359.90150	0.00002	294	g	sigma_g_plus
0	0	0	0	0	0	0	0	19	e	ortho	446.89078	0.00003	282	g	sigma_g_plus
0	0	0	0	0	0	0	0	21	e	ortho	543.26353	0.00002	274	g	sigma_g_plus
0	0	0	1	1	0	0	1	1	e	ortho	614.04436	0.00018	98	g	pi_g
0	0	0	1	1	0	0	1	2	f	ortho	618.77696	0.00013	133	g	pi_g

in other data sources (16AmFaHe_lyua07, 16AmFaHe_lyu08). Bands including $(0104^{0}1^{1})^{1}$ are not present in other data sources. We have swapped the labelling of these bands accordingly. All other bands from this dataset were included, with the exception of the single transition labelled 72BaGhNa_table2_c2_l32, which was not consistent with other datasets.

(3g) 17LyCa [23] provides a collection of data recorded in Grenoble using cavity ring down spectroscopy (CRDS) from several papers. 15LyVaCa (FTS15 in the notation of 17LyCa) [98], 16LyVaCa (FTS16) [101] and 17BeLyHu (FTS17) [102] were all already included as separate files in our dataset and so were removed from the 17LyCa [23] dataset. The remaining data, CRDS13 [120], CRDS14 [121] and CRDS16 [122] are all included in the final dataset with the tag '17LyCa'. See also comment (3l).

(3h) 07TrMaDa [86] contains a band labelled $2\nu_2+(\nu_4+3\nu_5)^{0}_{+}$. ℓ_4 and ℓ_5 were assigned in our dataset as +1 and -1 respectively, to be consistent with the labelling of 16AmFaHe_kep96.

(3i) Full data for 16KaNaVa [88] was provided in digital format by the corresponding author (private communication, Juho Karhu).

(3j) 77BaGhNa_table3_l205 of 77BaGhNa [92] is not compatible with the same transition in two other sources.

(3k) 16AmFaHe_amy11 [97] includes a band $((1000^{0}6^{6})^{6}$ - $(0000^{0}0^{0})^{0})$ which has transitions from $J=0$ to $J=10, 11, 12$. These are not physical and so have been removed from the dataset. There is one other transition which we removed as we found it to be inconsistent with the other datasets.

(3l) There has been some changes in the authors' approach to labelling levels between 15LyVaCa [98] and 17LyCa [23], see comment (3g) (Alain Campargue, private communication). This was partly to allow all bands to have unique labelling, as duplicate labels were provided in 15LyVaCa as indicated by ** or * superscripts. We have relabelled these bands to fit with other data sources, for example 16AmFaHe_amy11 [97]. We have been informed by the authors of 17LyCa that they are currently making amendments to their published dataset (Alain Campargue, private communication). Table 7 summarises the changes in labelling between 15LyVaCa, the current version of 17LyCa_FTS15 (see supplementary data of Lyulin and Campargue [23]) and this work.

(3m) 02VaElBr [100] is missing one band labelling in the footnote to their Table 4. The missing label for the penultimate level is $I=(v_1v_2v_3v_4^{l_4}v_5^{l_5})^{K}=(0020^{0}1^{1})^{1}$. Full data for this source was provided in digital format by the corresponding author (Jean Vander Auwera, private communication).

(3n) 16LyVaCa [101] has duplicate lines in the $(1110^{0}0^{0})^{0}$ band. Those which are inconsistent with other sources were removed and thus not included in the final data set for the MARVEL analysis. It is possible that they should be reassigned.

(3o) The assignments given for the band labelled $(0122^{0}2^{0})^{0}$ - $(0000^{0}0^{0})^{0}$ in 89HeHuVe [103] require the upper state to have the parity of an *f*-level, which is unphysical if both ℓ_4=0 and ℓ_5=0. There can be no *e*/*f* splitting in this case. We assumed this upper state should be labelled $(0122^{2}2^{-2})^{0}$. We have amended and included these reassigned transitions in our dataset.

(3p) Table 1 of 93SaKa [104] has duplicates for the $e\leftrightarrow e$ transitions in the $(2021^{1}0^{0})^{1}$ - $(0000^{0}1^{1})^{1}$ vibrational band. Those which are inconsistent with other sources were removed and thus not included in the final data set.

(3q) 92SaKa [106] contains some duplicate lines which have been assigned identical quantum numbers. Those transitions which are inconsistent with other sources were removed and thus not included in the final data set.

(3r) 94SaSeKa [107] gives two tables of data but only one is assigned with vibrational quantum numbers, so data from the other table were not considered in this study.

3.2. General comments

A number of general issues had to be dealt with before consistent rovibrational data could be obtained.

(1) 16AmFaHe [22] released a collation and analysis of experimental data in the middle of our collation and analysis stage. The entire database was formatted into MARVEL format so it could subsequently be run through the software and combined with the other experimental sources referenced in this paper. Some of the experimental sources featured in the 16AmFaHe database paper had already been collated and formatted to MARVEL format prior to its publication. These are 03JaMaDa [65], 91KaHeDi [52], 06LyPeMa [74], 07LyPeGu [82], 82RiBaRa [6], 02VaElBr [100] and 00MoDuJa [95]. We used a MARVEL format version of 16AmFaHe's compilation to compare to our data, as a further check to validate data had been digitised and formatted correctly; the versions included in the present study come from the original datasets for these papers. A few of the sources that were cited in 16AmFaHe were not included in our final dataset. There were 0 transitions in 16AmFaHe from

Table 9
Vibrational energy levels (cm^{-1}) from MARVEL analysis.

$(v_1v_2v_3v_4^{\ell_4}v_5^{\ell_5})^K$	e/f	State	MARVEL Energy (cm^{-1})	Uncertainty (cm^{-1})	NumTrans
$(0000^00^0)^0$	e	para	0.000000	0.000050	85
$(0002^00^0)^0$	e	para	1230.390303	0.000559	11
$(0001^11^{-1})^0$	e	ortho	1328.073466	0.000319	19
$(0001^11^{-1})^0$	f	para	1340.550679	0.001551	9
$(0000^02^0)^0$	e	para	1449.112363	0.001189	10
$(0100^00^0)^0$	e	para	1974.316617	0.006000	1
$(0003^11^{-1})^0$	e	ortho	2560.594937	0.002000	3
$(0002^22^{-2})^0$	e	para	2648.014468	0.004000	1
$(0001^13^{-1})^0$	e	ortho	2757.797907	0.001897	3
$(0000^04^0)^0$	e	para	2880.220077	0.004000	1
$(0101^11^{-1})^0$	e	ortho	3281.899025	0.001744	5
$(0010^00^0)^0$	e	ortho	3294.839579	0.001903	4
$(0101^11^{-1})^0$	f	para	3300.635590	0.007682	2
$(1000^00^0)^0$	e	para	3372.838987	0.016000	1
$(0103^11^{-1})^0$	e	ortho	4488.838166	0.001200	2
$(0012^00^0)^0$	e	ortho	4508.012219	0.002666	4
$(0102^22^{-2})^0$	f	ortho	4599.774669	0.003905	2
$(0011^11^{-1})^0$	e	para	4609.341046	0.005902	3
$(0011^11^{-1})^0$	f	ortho	4617.925870	0.005083	4
$(1001^11^{-1})^0$	e	ortho	4673.631058	0.001789	3
$(1001^11^{-1})^0$	f	para	4688.846488	0.011400	1
$(0101^13^{-1})^0$	e	ortho	4710.739822	0.018000	1
$(0010^02^0)^0$	e	ortho	4727.069907	0.001193	3
$(1000^02^0)^0$	e	para	4800.137287	0.000600	1
$(0201^11^{-1})^0$	e	ortho	5230.229286	0.010000	1
$(0110^00^0)^0$	e	ortho	5260.021842	0.003328	2
$(0103^13^{-1})^0$	e	ortho	5893.260496	0.010000	1
$(1001^13^{-1})^0$	e	ortho	6079.693064	0.003714	2
$(0010^04^0)^0$	e	ortho	6141.127536	0.010000	1
$(0112^00^0)^0$	e	ortho	6449.106486	0.006000	1
$(1102^00^0)^0$	e	para	6513.991447	0.008000	1
$(1010^00^0)^0$	e	ortho	6556.464783	0.000100	4
$(1101^11^{-1})^0$	e	ortho	6623.139603	0.011915	2
$(0110^02^0)^0$	e	ortho	6690.577636	0.012000	1
$(2000^00^0)^0$	e	para	6709.021187	0.003714	2
$(1100^02^0)^0$	e	para	6759.239077	0.010000	1
$(0114^00^0)^0$	e	ortho	7665.441780	0.010000	1
$(0022^00^0)^0$	e	para	7686.078947	0.002000	1
$(0204^22^{-2})^0$	e	para	7707.277687	0.004000	1
$(1012^00^0)^0$	e	ortho	7732.793472	0.005291	4
$(0203^33^{-3})^0$	e	ortho	7787.324394	0.010000	1
$(0021^11^{-1})^0$	e	ortho	7805.004672	0.001876	3
$(1103^11^{-1})^0$	e	ortho	7816.006736	0.010000	1
$(1011^11^{-1})^0$	f	ortho	7853.277113	0.012000	1
$(1010^02^0)^0$	e	ortho	7961.820133	0.007660	3
$(2001^11^{-1})^0$	e	ortho	7994.394918	0.002578	2
$(2001^11^{-1})^0$	f	para	8001.204086	0.009877	2
$(2000^02^0)^0$	e	para	8114.362883	0.003705	3
$(1100^04^0)^0$	e	para	8164.554028	0.008000	1
$(1110^00^0)^0$	e	ortho	8512.056241	0.000429	3
$(1201^11^{-1})^0$	e	ortho	8556.589655	0.010000	1
$(1201^11^{-1})^0$	f	para	8570.322888	0.010000	1
$(2100^00^0)^0$	e	para	8661.149087	0.010000	1
$(0300^04^0)^0$	e	para	8739.814487	0.010000	1
$(0310^00^0)^0$	e	ortho	9151.727686	0.010000	1
$(0030^00^0)^0$	e	ortho	9639.863579	0.015435	2
$(1112^00^0)^0$	e	ortho	9668.161468	0.015435	2
$(0122^22^{-2})^0$	f	ortho	9741.622286	0.030000	1
$(0121^11^{-1})^0$	e	ortho	9744.541486	0.030000	1
$(2010^00^0)^0$	e	ortho	9835.173105	0.015435	2
$(1030^00^0)^0$	e	ortho	12675.677286	0.001000	1
$(3010^00^0)^0$	e	ortho	13033.293786	0.010000	1
$(2210^00^0)^0$	e	ortho	13713.845686	0.006000	1

[108] (abb96), [109] (eli98) or [54] (drou11). The data for Drouin and Yu [54] were taken from the original paper (see 11DrYu in Table 5), but there was no data obviously available in the original papers for the other two sources. We have tried to keep the quantum number labelling consistent with that of 16AmFaHe as much as possible (see the next comment for an exception). Some other sources were labelled in order to make them consistent, in particular those cases were ℓ_4 and ℓ_5 were not defined in the original source.

(2) Many of the ℓ_4 and ℓ_5 assignments were inconsistent between different sources, were not given in the original data (often only $K = |\ell_4 + \ell_5|$ is given) or were inconsistent between data in the same dataset. Examples include the bands with upper energies labelled $(v_1v_2v_3v_4^{\ell_4}v_5^{\ell_5})^K = (0002^*1^*)^1$, $(1102^*1^*)^1$ or $(0102^*1^*)^1$ in

Table 10
Comparison of pure rotational levels with those of 16AmFaHe [22] and 17LyPe [24].

J	This work	Uncertainty	16AmFaHe	Difference	17LyPe	Difference	State
1	2.35329	0.00003	2.353286417	0	2.3533	0.00001	ortho
2	7.05982	0.00003	7.05982021	0	7.0598	−0.00002	para
3	14.11952	0.00002	14.119523294	0.00001	14.1195	−0.00002	ortho
4	23.53228	0.00003	23.532278547	0	23.5322	−0.00008	para
5	35.29793	0.00002	35.297929811	0	35.2978	−0.00013	ortho
6	49.41629	0.00003	49.416281896	−0.00001	49.4161	−0.00019	para
7	65.88709	0.00002	65.887100587	0	65.8869	−0.0002	ortho
8	84.71012	0.00002	84.710112648	−0.00001	84.7098	−0.00032	para
9	105.88501	0.00002	105.885005832	0	105.8846	−0.00041	ortho
10	129.41144	0.00003	129.411428888	−0.00001	129.411	−0.00044	para
11	155.28899	0.00002	155.28899157	0.00001	155.2885	−0.00049	ortho
12	183.51727	0.00003	183.517264652	−0.00001	183.5167	−0.00057	para
13	214.09576	0.00002	214.095779933	0.00002	214.0951	−0.00066	ortho
14	247.02403	0.00003	247.024030258	0	247.0233	−0.00073	para
15	282.30144	0.00002	282.301469525	0.00003	282.3007	−0.00074	ortho
16	319.92751	0.00003	319.927512702	0	319.9266	−0.00091	para
17	359.90149	0.00002	359.901535847	0.00004	359.9006	−0.0009	ortho
18	402.22287	0.00003	402.22287612	0.00001	402.2219	−0.00097	para
19	446.89078	0.00003	446.890831804	0.00006	446.8898	−0.00098	ortho
20	493.90464	0.00003	493.904662324	0.00002	493.9036	−0.00104	para
21	543.26353	0.00002	543.263588267	0.00006	543.2625	−0.00103	ortho
22	594.96668	0.00004	594.966791406	0.00011	594.9657	−0.00098	para
23	649.01328	0.00003	649.013414717	0.00014	649.0123	−0.00098	ortho
24	705.40237	0.00004	705.402562408	0.00019	705.4015	−0.00087	para
25	764.13315	0.00003	764.133299944	0.00015	764.1322	−0.00095	ortho
26	825.20439	0.00004	825.204654067	0.00026	825.2037	−0.00069	para
27	888.61531	0.00003	888.615612828	0.00031	888.6147	−0.00061	ortho
28	954.36496	0.00005	954.365125617	0.00017	954.3642	−0.00076	para
29	1022.45167	0.00003	1022.452103183	0.00044	1022.4513	−0.00037	ortho
30	1092.87513	0.00005	1092.875417676	0.00029	1092.8747	−0.00043	para
31	1165.63343	0.00004	1165.633902667	0.00048	1165.6333	−0.00013	ortho
32	1240.72592	0.00017	1240.726353188	0.00043	1240.7259	−0.00002	para
33	1318.15099	0.00011	1318.151525765	0.00054	1318.1512	0.00021	ortho
34	1397.90769	0.00023	1397.908138445	0.00045	1397.908	0.00031	para
35	1479.99435	0.00007	1479.994870843	0.00053	1479.9949	0.00055	ortho
36	1564.40979	0.00026	1564.410364167	0.00057	1564.4105	0.00071	para
37	1651.15189	0.00017	1651.153221265	0.00134	1651.1535	0.00161	ortho
38	1740.22038	0.00037	1740.222006657	0.00163	1740.2225	0.00212	para
39	1831.61393	0.00026	1831.615246582	0.00132	1831.6159	0.00197	ortho
40	1925.33058	0.00074	1925.331429031	0.00085	1925.3322	0.00162	para
41	2021.36757	0.00043	2021.369003793	0.00144	2021.3699	0.00233	ortho
42	2119.72439	0.0006	2119.726382499	0.00199	2119.7273	0.00291	para
43	2220.40059	0.00057	2220.401938666	0.00134	2220.4029	0.0023	ortho
44	2323.39201	0.00127	2323.394007739	0.002	2323.395	0.00299	para
45	2428.69912	0.00135	2428.70088714	0.00177	2428.7018	0.00268	ortho
46	2536.31702	0.00103	2536.320836316	0.00382	2536.3217	0.00468	para
47	2646.25026	0.00128	2646.252076785	0.00182	2646.2527	0.00244	ortho
48	2758.49217	0.00142	2758.492792187	0.00062	2758.4931	0.00093	para
49	2873.03874	0.00194	2873.041128336	0.00239	2873.0411	0.00236	ortho
50	2989.89046	0.00175	2989.895193269	0.00473	2989.8947	0.00424	para
51	3109.04649	0.00148	3109.0530573	0.00657	3109.0519	0.00541	ortho
52	3230.50478	0.00124	3230.512753073	0.00797	3230.5108	0.00602	para
53	3354.26378	0.00224	3354.272275619	0.0085	3354.2694	0.00562	ortho
54	3480.32661	0.0025	3480.329582411	0.00297	3480.3256	−0.00101	para
55	3608.67187	0.0025	3608.682593419	0.01073	3608.6772	0.00533	ortho
56	3739.32523	0.00118	3739.329191172	0.00396	3739.3223	−0.00293	para
57	3872.25528	0.00208	3872.267220814	0.01193	3872.2585	0.0032	ortho
58	4007.49264	0.0017	4007.494490165	0.00185	4007.4836	−0.00904	para
59	4144.99542	0.00118	4145.008769784	0.01335	4144.9955	0.00008	ortho
60	4284.80143	0.00181	4284.807793029	0.00636	4284.7918	−0.00963	para
61	4426.87718	0.00154	4426.889256124	0.01206	4426.8701	−0.0071	ortho
62	4571.24409	0.00142	4571.25081822	0.00673	4571.2281	−0.01599	para
63	4717.87442	0.00142	4717.890101462	0.01569	4717.8635	−0.01092	ortho
64	4866.79028	0.00232	4866.804691055	0.01441	4866.7736	−0.01668	para
65	5017.97095	0.00168	5017.992135336	0.02119	5017.9561	−0.01485	ortho
66	5171.43923	0.00366	5171.449945837	0.01072	5171.4085	−0.03073	para
67	5327.14526	0.00195	5327.175597358	0.03034	5327.128	−0.01726	ortho
69	5645.38676	0.003	5645.420139428	0.03338	5645.3585	−0.02826	ortho

16AmFaHe. Using simple combination differences, with the known lower value and given transition wavenumber, more than one value was found for the upper energy. We assume this duplication of quantum numbers for different states is due to the different method of analysis used in 16AmFaHe, which does not require a completely unique set. For example, for the upper level $(1102^21^{-1})^1$, J=2, *e*, there are two transitions which give as upper energy level of 7212.93 cm^{-1} (from 16AmFaHe_kep96) and three that give 7235.29 cm^{-1} (from 16AmFaHe_vda02 and 16AmFaHe_rob08). These same two energies can be found in multiple other sources (07TrMaDa, 15LyVaCa, 77BaGhNa, 02VaElBr), but the ℓ_4 and ℓ_5 assignment was inconsistent for states of the same upper energy. The decision was made to batch them together and assign the first energy level (7212.94 cm^{-1} in this example) as $(1102^21^{-1})^1$ and the second (7235.29 cm^{-1} in this example) as $(1102^01^1)^1$. The same logic was applied to other bands with $K = |\ell_4 + \ell_5|$=1.

(3) The *e*/*f* notation (see Section 2.2) was mostly specified in experimental papers, but some required additional investigation in order to assign them in such a way as to be consistent with other papers. The *c*/*d* notation in [45], for example, is analogous to the *e*/*f* notation used in this work.

(4) All transitions which were considered but not processed in the final dataset are labelled with _ct at the end of the reference and have a minus sign in front of the transition frequency, at the start of the file. MARVEL software ignores any line with a negative wavenumber.

3.3. Other comments

The following are sources of the $^{12}C_2H_2$ data in the HITRAN database ([66,123–125]): 16AmFaHe_gom09 [62], 16AmFaHe_gom10 [61], 96NaLaAw [96], 05EdBaMa [93], 16AmFaHe_lyua07 [82], 16AmFaHe_jac07 [69], 16AmFaHe_jac09 [99], 00Vander [63], 02HaVa [91], 03JaMaDab [66], 16AmFaHe_kab91 [52], 72Pliva [45], 03JaMaDa [65], 82RiBaRa [6], and 16AmFaHe_vda93 [71].

4. Results

The MARVEL website (http://kkrk.chem.elte.hu/marvelonline/marvel_full.php) has a version of MARVEL which can be run online. The variable NQN (number of quantum numbers) is 11 in the case of acetylene, given in Table 1. These quantum numbers are required for both the lower and upper levels, as illustrated in Table 4.

All energies are measured from the zero point energy (ZPE). This is the energy of the ground rovibrational state, which is given a relative energy of zero and is included in the *para* set of energy levels. The *ortho* set of energies therefore needs a 'magic number' to be added to all the MARVEL *ortho*-symmetry energies. Here the magic number was taken as the ground vibrational $(0000^00^0)^0$, J = 1 state of 16AmFaHe [22] who determined the value of 2.3532864 cm^{-1}, see Table 10 below. The output for the *ortho* energies in the supplementary data, and the extract of the output file in Table 8, all have this magic number added. The *para* component of the spectroscopic network does not require a magic number as it contains the ground rovibrational level, $(0000^00^0)^0$, $J = 0$. There are a small number (284 for *ortho* and 119 for *para*) of energy levels which are not joined to the two principal components (PCs) of the network. If more experimental transitions became available in the future it would be possible to link these to the PCs.

A total of 37,813 transitions were collated and considered (20,717 *ortho* and 17,096 *para*) from the data sources detailed in Section 3. Of those 607 were found to be inconsistent with others (353 *ortho* and 254 *para*) and thus removed from the final data set, leaving a total of 37,206 transitions used as input into MARVEL (20,364 *ortho* and 16,842 *para*). A plot of energy as a function of rotational quantum number, J, was made for each vibrational band as a check that quantum numbers had been assigned consistently. Figs. 1 and 2 show this for each vibrational band, for the *ortho* and *para* states respectively. Figs. 3 and 4 illustrate the *ortho* and *para* spectroscopic networks, respectively. The nodes are energy levels and the edges the transitions between them. Each consists of a large main network with a series of smaller networks currently unattached. Different algorithms can be used to present the experimental spectroscopic networks of $^{12}C_2H_2$; Fig. 5, for example, gives alternative representations of the structure. They highlight the intricate relationships between different energy levels and illustrate how the variety of sources collated in this work link together. We note that the inclusion of transitions intensities as weights in the spectroscopic network can aid in the determination of transitions which should preferentially be investigated in new experiments [28].

Table 9 gives the vibrational (J = 0) energies resulting from the MARVEL analysis, with associated uncertainty, vibrational assignment and the number of transitions (NumTrans) which were linked to the particular energy level. The higher the number of transitions the more certainty can be given to the energy value. See comment (3o) of Section 3.1 relating to the band $(0122^22^{-2})^0$ which may not have the correct assignment.

5. Comparison to other derived energy levels

Table 10 compares our rotational energy levels for the vibrational ground state, which are determined up to $J = 69$, with those obtained by 16AmFaHe [22] from an effective Hamiltonian fit to the observed data. In general the agreement is excellent. However, for the highest few levels with $J \geq 55$ we find differences which are significantly larger than our uncertainties; our levels are systematically below those of 16AmFaHe. This suggests that the effective Hamiltonian treatment used by 16AmFaHe becomes unreliable for these high J levels. It should be noted that the data relating to these highly excited levels originate from 16AmFaHe_amy9, a high-temperature experiment which has not been reproduced elsewhere; see comment (3d), Section 3.1. It is interesting to note that a further comparison with rotational energies extrapolated as part of 17LyPe's ASD-1000 spectroscopic databank [24], also given in Table 10, yields differences of approximately the same magnitude but, in contrast, consistently lower than our work.

The supplementary data from 17LyCa [23] contains lower energy levels, frequency and assignments, from which upper energy levels can be calculated. Fig. 6 gives the differences between the energies given in 17LyCa and this work as a function of J. The vast majority are within 0.005 cm^{-1}. Note that the difference in labelling of some bands has been taken into account when comparisons are made (see comment (3l) in Section 3.1 and comment (2) in Section 3.2).

The energy levels given as supplementary data in annex 5 of 16AmFaHe [22] are separated into polyads which are characterised by a small number of quantum numbers: $N_{rm\nu} = 5\nu_1 + 3\nu_2 + 5\nu_3 + \nu_4 + \nu_5$, J, *e*/*f* symmetry and *u*/*g* symmetry. As there are more than one state defined by these quantum numbers, the only comparison that was possible to make was to match these and find the closest energy value within these bounds. As such, we cannot be certain that bands have been matched correctly. 17LyCa compared what they could against 16AmFaHe's data but also could not find a reliable way to determine unambiguously which energy of each polyad block corresponds to their energy levels. Fig. 7 gives the difference between the energies in this work and those matched with 16AmFaHe as a function of rotational angular momentum quantum number, J. 6160 out of the 11154 energies differ by less than

0.01 cm^{-1}. However, this leaves 4994 energies with a difference of higher than 0.01 cm^{-1}. 2176 of these energies also appear in 17LyCa, so a comparison could be made between the three. Only 7 of the energies in the 17LyCa dataset are closer to 16AmFaHe than this work, and of those all are within 0.02 cm^{-1} with this work.

It should be noted, however, that the differences between this work and 16AmFaHe are largest for those energy levels with low values of NumTrans (the number of transitions that link the energy state to other energies within the dataset); see Fig. 8. The vast majority of energy levels which only have one transition are not in the 17LyCa dataset. Many of these transitions came from the data source 16AmFaHe_amy09; see comment (3d) in Section 3.1. It would be of use to have more experimental data on transitions to these levels in order to confirm their validity. The entire band $(0122^22^{-2})^0$ has differences of over 900 cm^{-1} in comparison to the matched values in 16AmFaHe. This indicates that this band has been misassigned (see comment (3o) in Section 3.1). We are uncertain currently as what it should be reassigned to. We have excluded this band from Figs. 7 and 8.

It should be made clear, as mentioned above, that those energy levels present in the input data which are only linked to the main principal components of the spectroscopic network by one transition should be treated with caution; this number is given as a parameter in the third to last column of the output files included in the supplementary data. The number of transitions determining an energy level can be used, along with the uncertainties, as an indication of the reliability of each energy level. Note, finally, that MARVEL only processes data given as input; it does not extrapolate to higher excitations.

6. Conclusions

A total of 37813 measured experimental transitions from 61 publications have been considered in this work. From this 6013 *ortho* and 5200 *para* energy levels have been determined using the Measured Active Rotational-Vibrational Energy Levels (MARVEL) technique. These results have been compared with alternative compilations based on the use of effective Hamiltonians. An *ab initio* high temperature linelist for acetylene is in preparation as part of the ExoMol project [126], for which this data will be used in the process of validation of theoretical calculations.

A significant part of this work was performed by pupils from Highams Park School in London, as part of a project known as ORBYTS (Original Research By Young Twinkle Scientists). The MARVEL study of TiO [33] was also performed as part of the ORBYTS project and further studies on other key molecules will be published in due course. A paper discussing our experiences of performing original research in collaboration with school children will be published elsewhere [127].

Acknowledgments

We would like to thank Jon Barker, Fawad Sheikh, and Sheila Smith from Highams Park School for continued support and enthusiasm. Jean Vander Auwera, Juho Karhu, Alain Campargue, Oleg Lyulin and Michel Herman are thanked for helping with our queries and providing digital versions of published data where necessary. We are grateful to Laura McKemmish for helpful discussions and advice. We are also grateful to the authors of all the experimental sources analysed in this work (and apologies to any we may have missed) for the high accuracy and copious amounts of acetylene data they have made available to the scientific community over the years. This work was supported by STFC Project ST/J002925, by NKFIH by grant no. 119658, the ERC under Advanced Investigator Project 267219 and the COST action MOLIM: Molecules in Motion (CM1405). We would like to thank the reviewers of this paper for useful comments and suggestions, and to Michel Herman, Badr Amyay, Oleg Lyulin, and Alain Campargue for interesting discussions.

Supplementary material

Supplementary material associated with this article can be found, in the online version, at 10.1016/j.jqsrt.2017.08.018.

References

[1] Gaydon A. The spectroscopy of flames. springer science & business media; 2012.
[2] Metsälä M, Schmidt FM, Skytta M, Vaittinen O, Halonen L. Acetylene in breath: background levels and real-time elimination kinetics after smoking. J Breath Res 2010;4:046003. doi:10.1088/1752-7155/4/4/046003.
[3] Dhanoa H, Rawlings JMC. Is acetylene essential for carbon dust formation? Mon Not Soc 2014;440:1786–93. doi:10.1093/mnras/stu401.
[4] Ridgway ST, Hall DNB, Kleinmann SG, Weinberger DA, Wojslaw RS. Circumstellar acetylene in the infrared spectrum of IRC+10216. Nature 1976;264:345–6.
[5] Bilger C, Rimmer P, Helling C. Small hydrocarbon molecules in cloud-forming brown dwarf and giant gas planet atmospheres. Mon Not R Astron Soc 2013;435:1888–903. doi:10.1093/mnras/stt1378.
[6] Rinsland CP, Baldacci A, Rao KN. Acetylene bands observed in carbon stars - a laboratory study and an illustrative example of its application to IRC+10216. Astrophys J Suppl 1982;49:487–513. doi:10.1086/190808.
[7] Gautschy-Loidl R, Hofner S, Jorgensen U, Hron J. Dynamic model atmospheres of AGB stars - IV. A comparison of synthetic carbon star spectra with observations. Astron Astrophys 2004;422:289–306. doi:10.1051/0004-6361:20035860.
[8] Oremland RS, Voytek MA. Acetylene as fast food: implications for development of life on anoxic primordial earth and in the outer solar system. Astrobiology 2008:45–58. doi:10.1089/ast.2007.0183.
[9] Brooke TY, Tokunaga AT, Weaver HA, Crovisier J, BockeleeMorvan D, Crisp D. Detection of acetylene in the infrared spectrum of comet Hyakutake. Nature 1996;383:606–8. doi:10.1038/383606a0.
[10] Tsiaras A, Rocchetto M, Waldmann IP, Tinetti G, Varley R, Morello G, et al. Detection of an atmosphere around the super-earth 55 Cancri e. Astrophys J 2016;820:99. doi:10.3847/0004-637X/820/2/99.
[11] Herman M. The acetylene ground state saga. Mol Phys 2007;105:2217–41. doi:10.1080/00268970701518103.
[12] Didriche K, Herman M. A four-atom molecule at the forefront of spectroscopy, intramolecular dynamics and astrochemistry: acetylene. Chem Phys Lett 2010;496:1–7. doi:10.1016/j.cplett.2010.07.031.
[13] Herman M. High-resolution infrared spectroscopy of acetylene: theoretical background and research trends. John Wiley & Sons, Ltd; 2011. p. 1993–2026. doi:10.1002/9780470749593.hrs101.
[14] Bramley MJ, Handy NC. Efficient calculation of rovibrational eigenstates of sequentially bonded 4-atom molecules. J Chem Phys 1993;98:1378–97. doi:10.1063/1.464305.
[15] Schwenke DW. Variational calculations of rovibrational energy levels and transition intensities for tetratomic molecules. J Phys Chem 1996;100:2867–84. doi:10.1021/jp9525447.
[16] Kozin IN, Law MM, Tennyson J, Hutson JM. Calculating energy levels of isomerizing tetraatomic molecules: II. The vibrational states of acetylene and vinylidene. J Chem Phys 2005;122:064309.
[17] Xu DG, Li GH, Xie DQ, Guo H. Full-dimensional quantum calculations of vibrational energy levels of acetylene (HCCH) up to 13,000 cm^{-1}. Chem Phys Lett 2002;365:480–6. doi:10.1016/S0009-2614(02)01503-8.
[18] Xu DG, Guo H, Zou SL, Bowman JM. A scaled ab initio potential energy surface for acetylene and vinylidene. Chem Phys Lett 2003;377:582–8. doi:10.1016/S0009-2614(03)01184-9.
[19] Urru A, Kozin IN, Mulas G, Braams BJ, Tennyson J. Rovibrational spectra of C_2H_2 based on variational nuclear motion calcalculations. Mol Phys 2010;108:1973–90.
[20] Tennyson J, Yurchenko SN. Exomol: molecular line lists for exoplanet and other atmospheres. Mon Not R Astron Soc 2012;425:21–33. doi:10.1111/j.1365-2966.2012.21440.x.
[21] Tennyson J, Yurchenko SN, Al-Refaie AF, Barton EJ, Chubb KL, Coles PA, et al. The ExoMol database: molecular line lists for exoplanet and other hot atmospheres. J Mol Spectrosc 2016;327:73–94. doi:10.1016/j.jms.2016.05.002.
[22] Amyay B, Fayt A, Herman M, Auwera JV. Vibration-rotation spectroscopic database on acetylene, $X\ ^1\sum_g^{+12}C_2H_2$. J Phys Chem Ref Data 2016;45:023103. doi:10.1063/1.4947297.
[23] Lyulin OM, Campargue A. An empirical spectroscopic database for acetylene in the regions of 5850.6341 cm^{-1} and 7000.9415 cm^{-1}. J Quant Spectrosc Radiat Transf 2017. doi:10.1016/j.jqsrt.2017.01.036.
[24] Lyulin OM, Perevalov VI. ASD-1000: High-resolution, high-temperature acetylene spectroscopic databank. J Quant Spectrosc Radiat Transf 2017;201:94–103. doi:10.1016/j.jqsrt.2017.06.032.

[25] Lyulin OM, Perevalov VI. Global modeling of vibration-rotation spectra of the acetylene molecule. J Quant Spectrosc Radiat Transf 2016;177:59–74. doi:10.1016/j.jqsrt.2015.12.021.

[26] Furtenbacher T, Császár AG, Tennyson J. MARVEL: measured active rotational-vibrational energy levels. J Mol Spectrosc 2007;245:115–25.

[27] Furtenbacher T, Császár AG. MARVEL: measured active rotational-vibrational energy levels. II. Algorithmic improvements. J Quant Spectrosc Radiat Transf 2012;113:929–35.

[28] Császár AG, Furtenbacher T. Spectroscopic networks. J Mol Spectrosc 2011;266:99–103. doi:10.1016/j.jms.2011.03.031.

[29] Császár AG, Furtenbacher T, Árendás P. Small molecules - big data. J Phys Chem A 2016;120:8949–69.

[30] Flaud J-M, Camy-Peyret C, Maillard J-P. Higher rovibrational levels of H_2O deduced from high-resolution oxygen-hydrogen flame spectra between 2800–6200 cm^{-1}. Mol Phys 1976;32:499–521. doi:10.1080/00268977600103251.

[31] Watson JK. Robust weighting in least-squares fits. J Mol Spectrosc 2003;219(2):326–8. doi:10.1016/S0022-2852(03)00100-0.

[32] Watson JKG. The use of term-value fits in testing spectroscopic assignments. J Mol Spectrosc 1994;165:283–90. doi:10.1006/jmsp.1994.1130.

[33] McKemmish LK, Masseron T, Sheppard S, Sandeman E, Schofield Z, Furtenbacher T, et al. MARVEL analysis of the measured high-resolution spectra of $^{48}Ti^{16}O$. Astrophys J Suppl 2017;228:15. doi:10.3847/1538-4365/228/2/15.

[34] Al Derzi AR, Furtenbacher T, Yurchenko SN, Tennyson J, Császár AG. MARVEL analysis of the measured high-resolution spectra of $^{14}NH_3$. J Quant Spectrosc Radiat Transf 2015;161:117–30. doi:10.1016/j.jqsrt.2015.03.034.

[35] Furtenbacher T, Coles PA, Tennyson J, Császár AG. Updated MARVEL energy levels for ammonia. J Quant Spectrosc Radiat Transf., (in preparation).

[36] Tennyson J, Bernath PF, Brown LR, Campargue A, Carleer MR, Császár AG, et al. IUPAC critical evaluation of the rotational-vibrational spectra of water vapor. Part i. energy levels and transition wavenumbers for $H_2{}^{17}O$ and $H_2{}^{18}O$. J Quant Spectrosc Radiat Transf 2009;110:573–96. doi:10.1016/j.jqsrt.2009.02.014.

[37] Tennyson J, Bernath PF, Brown LR, Campargue A, Carleer MR, Császár AG, et al. IUPAC critical evaluation of the rotational-vibrational spectra of water vapor. Part II. energy levels and transition wavenumbers for $HD^{16}O$, $HD^{17}O$, and $HD^{18}O$. J Quant Spectrosc Radiat Transf 2010;111:2160–84. doi:10.1016/j.jqsrt.2010.06.012.

[38] Tennyson J, Bernath PF, Brown LR, Campargue A, Carleer MR, Császár AG, et al. IUPAC critical evaluation of the rotational-vibrational spectra of water vapor. Part III. energy levels and transition wavenumbers for $H_2{}^{16}O$. J Quant Spectrosc Radiat Transf 2013;117:29–80. doi:10.1016/j.jqsrt.2012.10.002.

[39] Tennyson J, Bernath PF, Brown LR, Campargue A, Császár AG, Daumont L, et al. IUPAC critical evaluation of the rotational-vibrational spectra of water vapor. Part IV. energy levels and transition wavenumbers for $D_2{}^{16}O$, $D_2{}^{17}O$ and $D_2{}^{18}O$. J Quant Spectrosc Radiat Transf 2014;142:93–108. doi:10.1016/j.jqsrt.2014.03.019.

[40] Furtenbacher T, Dénes N, Tennyson J, Naumenko OV, Polyansky OL, Zobov NF, et al. The 2016 update of the IUPAC database of water energy levels. J Quant Spectrosc Radiat Transf, (in preparation).

[41] Furtenbacher T, Szidarovszky T, Fábri C, Császár AG. MARVEL analysis of the rotational–vibrational states of the molecular ions H_2D^+ and D_2H^+. Phys Chem Chem Phys 2013;15:10181–93.

[42] Furtenbacher T, Szidarovszky T, Mátyus E, Fábri C, Császár AG. Analysis of the rotational–vibrational states of the molecular ion H_3^+. J Chem Theory Comput 2013;9:5471–8.

[43] Furtenbacher T, Szabó I, Császár AG, Bernath PF, Yurchenko SN, Tennyson J. Experimental energy levels and partition function of the $^{12}C_2$ molecule. Astrophys J Suppl 2016;224(44). doi:10.3847/0067-0049/224/2/44.

[44] Brown JM, Hougen JT, Huber K-P, Johns JWC, Kopp I, Lefebvre-Brion H, et al. The labelling of parity doublet levels in linear molecules. J Mol Spectrosc 1975;55:500–3. doi:10.1016/0022-2852(75)90291-X.

[45] Plíva J. Spectrum of acetylene in the 5-micron region. J Mol Spectrosc 1972;44:145–64. doi:10.1016/0022-2852(72)90198-1.

[46] Winnewisser M, Winnewisser BP. Millimeter wave rotational spectrum of HCNO in vibrationally excited states. J Mol Spectrosc 1972;41(1):143–76. doi:10.1016/0022-2852(72)90129-4.

[47] Herman M, Lievin J, Auwera JV, Campargue A. Global and accurate vibration Hamiltonians from high-resolution molecular spectroscopy, 108. Wiley and Sons, Inc; 1999. of Adv Chem Phys, New York, NY.

[48] Herman M, Lievin J. Acetylene- from intensity alternation in spectra to ortho and para molecule. J Chem Educ 1982;59:17. doi:10.1021/ed059p17.

[49] Bunker PR, Jensen P. Molecular symmetry and spectroscopy. 2nd Edition. Ottawa: NRC Research Press; 1998.

[50] Tennyson J, Bernath PF, Brown LR, Campargue A, Császár AG, Daumont L, et al. A database of water transitions from experiment and theory (IUPAC technical report). Pure Appl Chem 2014;86:71–83. doi:10.1515/pac-2014-5012.

[51] Yu S, Drouin BJ, Pearson JC. Terahertz spectroscopy of the bending vibrations of acetylene $^{12}C_2H_2$. Astrophys J 2009;705:786–90. doi:10.1088/0004-637X/705/1/786.

[52] Kabbadj Y, Herman M, Dilonardo G, Fusina L, Johns JWC. The bending energy-levels of C_2H_2. J Mol Spectrosc 1991;150:535–65. doi:10.1016/0022-2852(91)90248-9.

[53] Amyay B, Herman M, Fayt A, Fusina L, Predoi-Cross A. High resolution FTIR investigation of $^{12}C_2H_2$ in the FIR spectral range using synchrotron radiation. Chem Phys Lett 2010;491:17–19. doi:10.1016/j.cplett.2010.03.053.

[54] Drouin BJ, Yu S. Acetylene spectra near 2.6 THz. J Mol Spectrosc 2011;269:254–6. doi:10.1016/j.jms.2011.06.004.

[55] Jacquemart D, Lyulin OM, Perevalov VI. Recommended acetylene line list in the 20–240 cm^{-1} and 400–630 cm^{-1} regions: new measurements and global modeling. J Quant Spectrosc Radiat Transf. 2017 10.1016/j.jqsrt.2017.03.008.

[56] Hietanen J, Kauppinen J. High-resolution infrared-spectrum of acetylene in the region of the bending fundamental ν_5. Mol Phys 1981;42:411–23. doi:10.1080/00268978100100351.

[57] Weber M, Blass WE, Nadler S, Halsey GW, Maguire WC, Hillman JJ. Resonance effects in C_2H_2 near 13.7 μm. part h: the two quantum hotbands. Spectra Chimica Acta A 1993;49:1659–81. doi:10.1016/0584-8539(93)80124-S.

[58] Mandin JY, Dana V, Claveau C. Line intensities in the ν_5 band of acetylene $^{12}C_2H_2$. J Quant Spectrosc Radiat Transf 2000;67:429–46. doi:10.1016/S0022-4073(00)00010-8.

[59] Jacquemart D, Claveau C, Mandin JY, Dana V. Line intensities of hot bands in the 13.6 μmspectral region of acetylene $^{12}C_2H_2$. J Quant Spectrosc Radiat Transf 2001;69:81–101. doi:10.1016/S0022-4073(00)00063-7.

[60] Bell EE, Nielsen HH. The infra-red spectrum of acetylene. J Chem Phys 1950;18:1382–94. doi:10.1063/1.1747483.

[61] Gomez L, Jacquemart D, Lacome N, Mandin J-Y. New line intensity measurements for $^{12}C_2H_2$ around 7.7 μm and HITRAN format line list for applications. J Quant Spectrosc Radiat Transf 2010;111:2256–64. doi:10.1016/j.jqsrt.2010.01.031.

[62] Gomez L, Jacquemart D, Lacome N, Mandin JY. Line intensities of $^{12}C_2H_2$ in the 7.7 μm spectral region. J Quant Spectrosc Radiat Transf 2009;110:2102–14. doi:10.1016/j.jqsrt.2009.05.018.

[63] Auwera JV. Absolute intensities measurements in the $\nu_4 + \nu_5$ band of $^{12}C_2H_2$: analysis of Herman–Wallis effects and forbidden transitions. J Mol Spectrosc 2000;201:143–50. doi:10.1006/jmsp.2000.8079.

[64] Amyay B, Robert S, Herman M, Fayt A, Raghavendra B, Moudens A, et al. Vibration-rotation pattern in acetylene. II. Introduction of coriolis coupling in the global model and analysis of emission spectra of hot acetylene around 3 μm. J Chem Phys 2009;131:114301. doi:10.1063/1.3200928.

[65] Jacquemart D, Mandin JY, Dana V, Regalia-Jarlot L, Plateaux J, Decatoire D, et al. The spectrum of acetylene in the 5-μm region from new line-parameter measurements. J Quant Spectrosc Radiat Transf 2003;76:237–67. doi:10.1016/S0022-4073(02)00055-9.

[66] Jacquemart D, Mandin JY, Dana V, Claveau C, Auwera JV, Herman A, et al. The IR acetylene spectrum in HITRAN: update and new results. J Quant Spectrosc Radiat Transf 2003;82:363–82. doi:10.1016/S0022-4073(03)00163-8.

[67] Jacquemart D, Mandin JY, Dana V, Regalia-Jarlot L, Thomas X, Von der Heyden P. Multispectrum fitting measurements of line parameters for 5-μm cold bands of acetylene. J Quant Spectrosc Radiat Transf 2002;75:397–422. doi:10.1016/S0022-4073(02)00017-1.

[68] Bermejo D, Cancio P, Lonardo GD, Fusina L. High resolution raman spectroscopy from vibrationally excited states populated by a stimulated raman process: $2\nu_2 - \nu_2$ of $^{12}C_2H_2$ and $^{12}C_2H_2$. J Chem Phys 1998;108:7224–8. doi:10.1063/1.476140.

[69] Jacquemart D, Lacome N, Mandin JY, Dana V, Lyulin OM, Perevalov VI. Multispectrum fitting of line parameters for $^{12}C_2H_2$ in the 3.8-μm spectral region. J Quant Spectrosc Radiat Transf 2007;103:478–95. doi:10.1016/j.jqsrt.2006.06.008.

[70] Palmer KF, Mickelson ME, Rao KN. Investigations of several infrared bands of $^{12}C_2H_2$ and studies of the effects of vibrational rotational interactions. J Mol Spectrosc 1972;44:131–44. doi:10.1016/0022-2852(72)90197-X.

[71] Auwera JV, Hurtmans D, Carleer M, Herman M. The ν_3 fundamental in C_2H_2. J Mol Spectrosc 1993;157:337–57. doi:10.1006/jmsp.1993.1027.

[72] Dcunha R, Sarma YA, Job VA, Guelachvili G, Rao KN. Fermi coupling and ℓ-type resonance effects in the hot bands of acetylene: the 2650-cm^{-1} region. J Mol Spectrosc 1993;157:358–68. doi:10.1006/jmsp.1993.1028.

[73] Sarma YA, Dcunha R, Guelachvili G, Farrenq R, Devi VM, Benner DC, et al. Stretch-bend levels of acetylene - analysis of the hot bands in the 3300cm^{-1} region. J Mol Spectrosc 1995;173:574–84. doi:10.1006/jmsp.1995.1258.

[74] Lyulin OM, Perevalov VI, Mandin JY, Dana V, Jacquemart D, Regalia-Jarlot L, et al. Line intensities of acetylene in the 3-μm region: new measurements of weak hot bands and global fitting. J Quant Spectrosc Radiat Transf 2006;97:81–98. doi:10.1016/j.jqsrt.2004.12.022.

[75] Mandin JY, Jacquemart D, Dana V, Regalia-Jarlot L, Barbe A. Line intensities of acetylene at 3 μm. J Quant Spectrosc Radiat Transf 2005;92:239–60. doi:10.1016/j.jqsrt.2004.07.024.

[76] Sarma YA, Dcunha R, Guelachvili G, Farrenq R, Rao KN. Stretch-bend levels of acetylene - analysis of the hot bands in the 3800cm^{-1} region. J Mol Spectrosc 1995;173:561–73. doi:10.1006/jmsp.1995.1257.

[77] Bermejo D, Martinez RZ, Lonardo GD, Fusina L. High resolution raman spectroscopy from vibrationally excited states populated by a stimulated raman process. transitions from $\nu_2 = 1$ in $^{12}C_2H_2$ and $^{13}C_2H_2$. J Chem Phys 1999;111:519–24. doi:10.1063/1.479331.

[78] Lyulin OM, Perevalov VI, Mandin JY, Dana V, Gueye F, Thomas X, et al. Line intensities of acetylene: measurements in the 2.5-μm spectral region and global modeling in the $\Delta p = 4$ and 6 series. J Quant Spectrosc Radiat Transf 2007;103:496–523. doi:10.1016/j.jqsrt.2006.07.002.

[79] Girard V, Farrenq R, Sorokin E, Sorokina IT, Guelachvili G, Picque N. Acetylene weak bands at 2.5 μm from intracavity Cr^{2+}: ZnSe laser absorption observed with time-resolved fourier transform spectroscopy. Chem Phys Lett 2006;419:584–8. doi:10.1016/j.cplett.2005.12.029.

[80] Dcuhna R, Sarma YA, Guelachvili G, Farrenq R, Kou QL, Devi VM, et al. Analysis of the high-resolution spectrum of acetylene in the 2.4 μm region. J Mol Spectrosc 1991;148:213–25. doi:10.1016/0022-2852(91)90048-F.

[81] Baldacci A, Ghersetti S, Rao KN. Assignments of the $^{12}C_2H_2$ bands at 2.1–2.2 μm. J Mol Spectrosc 1972;41:222–5. doi:10.1016/0022-2852(72)90134-8.

[82] Lyulin OM, Perevalov VI, Gueye F, Mandin JY, Dana V, Thomas X, et al. Line positions and intensities of acetylene in the 2.2-μm region. J Quant Spectrosc Radiat Transf 2007;104:133–54. doi:10.1016/j.jqsrt.2006.08.018.

[83] Lyulin OM, Jacquemart D, Lacome N, Perevalov VI, Mandin JY. Line parameters of acetylene in the 1.9 and 1.7 μm spectral regions. J Quant Spectrosc Radiat Transf 2008;109:1856–74. doi:10.1016/j.jqsrt.2007.11.016.

[84] Keppler KA, Mellau GC, Klee S, Winnewisser BP, Winnewisser M, Pliva J, et al. Precision measurements of acetylene spectra at 1.4-1.7 μm recorded with 352.5-m pathlength. J Mol Spectrosc 1996;175:411–20. doi:10.1006/jmsp.1996.0047.

[85] Robert S, Herman M, Fayt A, Campargue A, Kassi S, Liu A, et al. Acetylene, $^{12}C_2H_2$: new CRDS data and global vibration-rotation analysis up to 8600 cm^{-1}. Mol Phys 2008;106:2581–605. doi:10.1080/00268970802620709.

[86] Tran H, Mandin JY, Dana V, Regalia-Jarlot L, Thomas X, Von der Heyden P. Line intensities in the 1.5-μm spectral region of acetylene. J Quant Spectrosc Radiat Transf 2007;108:342–62. doi:10.1016/j.jqsrt.2007.04.008.

[87] Lyulin OM, Perevalov VI, Tran H, Mandin JY, Dana V, Regalia-Jarlot L, et al. Line intensities of acetylene: new measurements in the 1.5-μm spectral region and global modelling in the $\triangle p = 10$ series. J Quant Spectrosc Radiat Transf 2009;110:1815–24. doi:10.1016/j.jqsrt.2009.04.012.

[88] Karhu J, Nauta J, Vainio M, Metsälä M, Hoekstra S, Halonen L. Double resonant absorption measurement of acetylene symmetric vibrational states probed with cavity ring down spectroscopy. J Chem Phys 2016;144:244201. doi:10.1063/1.4954159.

[89] Kou Q, Guelachvili G, Temsamani MA, Herman M. The absorption spectrum of C_2H_2 around $\nu_1 + \nu_3$ - energy standards in the 1.5 μm region and vibrational clustering. Can J Phys 1994;72:1241–50. doi:10.1139/p94-160.

[90] Twagirayezu S, Cich MJ, Sears TJ, Raven CPM, Hall GE. Frequency-comb referenced spectroscopy of ν_4- and ν_5-excited hot bands in the 1.5 μm spectrum of C_2H_2. J Mol Spectrosc 2015;316:64–71. doi:10.1016/j.jms.2015.06.010.

[91] Hachtouki RE, Auwera JV. Absolute line intensities in acetylene: the 1.5-μm region. J Mol Spectrosc 2002;216:355–62. doi:10.1006/jmsp.2002.8660.

[92] Baldacci A, Ghersetti S, Rao KN. Interpretation of the acetylene spectrum at 1.5 μm. J Mol Spectrosc 1977;68:183–94. doi:10.1016/0022-2852(77)90436-2.

[93] Edwards CS, Barwood GP, Margolis HS, Gill P, Rowley WRC. High-precision frequency measurements of the $\nu_1 + \nu_3$ combination band of $^{12}C_2H_2$ in the 1.5 μm region. J Mol Spectrosc 2005;234:143–8. doi:10.1016/j.jms.2005.08.014.

[94] Zolot AM, Giorgetta FR, Baumann E, Swann WC, Coddington I, Newbury NR. Broad-band frequency references in the near-infrared: accurate dual comb spectroscopy of methane and acetylene. J Quant Spectrosc Radiat Transf 2013;118:26–39. doi:10.1016/j.jqsrt.2012.11.024.

[95] Moss DB, Duan ZC, Jacobson MP, O'Brien JP, Field RW. Observation of coriolis coupling between $\nu_2 + 4\nu_4$ and $7\nu_4$ in acetylene $^1\Sigma_g^+$ by stimulated emission pumping spectroscopy. J Mol Spectrosc 2000;199:265–74. doi:10.1006/jmsp.1999.7994.

[96] Nakagawa K, deLabachelerie M, Awaji Y, Kourogi M. Accurate optical frequency atlas of the 1.5-μm bands of acetylene. J Opt Soc Am B 1996;13:2708–14. doi:10.1364/JOSAB.13.002708.

[97] Amyay B, Herman M, Fayt A, Campargue A, Kassi S. Acetylene, ($^{12}C_2H_2$): refined analysis of CRDS spectra around 1.52 μm. J Mol Spectrosc 2011;267:80–91. doi:10.1016/j.jms.2011.02.015.

[98] Lyulin OM, Auwera JV, Campargue A. The fourier transform absorption spectrum of acetylene between 7000 and 7500 cm^{-1}. J Quant Spectrosc Radiat Transf 2015;160:85–93. doi:10.1016/j.jqsrt.2015.03.018.

[99] Jacquemart D, Lacome N, Mandin JY, Dana V, Tran H, Gueye FK, et al. The IR spectrum of $^{12}C_2H_2$: line intensity measurements in the 1.4 μm region and update of the databases. J Quant Spectrosc Radiat Transf 2009;110:717–32. doi:10.1016/j.jqsrt.2008.10.002.

[100] Auwera JV, Hachtouki RE, Brown LR. Absolute line wavenumbers in the near infrared: $^{12}C_2H_2$ and $^{12}C^{16}O_2$. Mol Phys 2002;100:3563–76. doi:10.1080/00268970210162880.

[101] Lyulin OM, Auwera JV, Campargue A. The Fourier transform absorption spectrum of acetylene between 8280 and 8700 cm^{-1}. J Quant Spectrosc Radiat Transf 2016;177:234–40. doi:10.1016/j.jqsrt.2015.11.026.

[102] Béguier S, Lyulin OM, Hu S-M, Campargue A. Line intensity measurements for acetylene between 8980 and 9420 cm^{-1}. J Quant Spectrosc Radiat Transf 2017;189:417–20. doi:10.1016/j.jqsrt.2016.12.020.

[103] Herman M, Huet TR, Vervloet M. Spectroscopy and vibrational couplings in the $3\nu_3$ region of acetylene. Mol Phys 1989;66:333–53. doi:10.1080/00268978900100161.

[104] Sakai J, Katayama M. Diode laser spectroscopy of acetylene: the $2\nu_1 + 2\nu_3 + \nu_4 - \nu_5$ and $4\nu_1 - \nu_5$ interacting band system. J Mol Spectrosc 1993;157:532–5. doi:10.1006/jmsp.1993.1042.

[105] Herregodts F, Kerrinckx E, Huet TR, Auwera JV. Absolute line intensities in the $\nu_1 + 3\nu_3$ band of $^{12}C_2H_2$ by laser photoacoustic spectroscopy and fourier transform spectroscopy. Mol Phys 2003;101:3427–38. doi:10.1080/00268970310001632426.

[106] Sakai J, Katayama M. Diode laser spectroscopy of acetylene: $3\nu_3 + \nu_1 3$ region at 0.77 μm. J Mol Spectrosc 1992;154:277–87. doi:10.1016/0022-2852(92)90208-6.

[107] Sakai J, Segawa H, Katayama M. Diode laser spectroscopy of the $2\nu_1 + 2\nu_2 + \nu_3$ band of acetylene. J Mol Spectrosc 1994;164:580–2. doi:10.1006/jmsp.1994.1101.

[108] Temsamani MA, Herman M, Solina SAB, O'Brien JP, Field RW. Highly vibrationally excited $^{12}C_2H_2$ in the X $^1\Sigma_g^+$ state: complementarity of absorption and dispersed fluorescence spectra. J Chem Phys 1996;105:11357–9. doi:10.1063/1.472995.

[109] Idrissi MIE, Lievin J, Campargue A, Herman M. The vibrational energy pattern in acetylene (IV): updated global vibration constants for $^{12}C_2H_2$. J Chem Phys 1999;110:2074–86. doi:10.1063/1.477817.

[110] Plíva J. Molecular constants for the bending modes of acetylene $^{12}C_2H_2$. J Mol Spectrosc 1972;44:165–82. doi:10.1016/0022-2852(72)90199-3.

[111] Metsälä M, Yang S, Vaittinen O, Halonen L. Laser-induced dispersed vibration-rotation fluorescence of acetylene: spectra of ortho and para forms and partial trapping of vibrational energy. J Chem Phys 2002;117:8686–93. doi:10.1063/1.1513464.

[112] Metsälä M, Yang SF, Vaittinen A, Permogorov D, Halonen L. High-resolution cavity ring-down study of acetylene between 12260 and 12380 cm^{-1}. Chem Phys Lett 2001;346:373–8. doi:10.1016/S0009-2614(01)00945-9.

[113] Saarinen M, Permogorov D, Halonen L. Collision-induced vibration-rotation fluorescence spectra and rovibrational symmetry changes in acetylene. J Chem Phys 1999;110:1424–8. doi:10.1063/1.478017.

[114] Jungner P, Halonen L. Laser induced vibration-rotation fluorescence and infrared forbidden transitions in acetylene. J Chem Phys 1997;107:1680–2. doi:10.1063/1.474521.

[115] Zhan XW, Halonen L. High-resolution photoacoustic study of the $\nu_1 + 3\nu_3$ band system of acetylene with a titanium-sapphire ring laser. J Mol Spectrosc 1993;160:464–70. doi:10.1006/jmsp.1993.1193.

[116] Zhan XW, Vaittinen O, Halonen L. High-resolution photoacoustic study of acetylene between 11500 and 11900cm^{-1} using a titanium-sapphire ring laser. J Mol Spectrosc 1993;160:172–80. doi:10.1006/jmsp.1993.1165.

[117] Zhan X-W, Vaittinen O, Kauppi E, Halonen L. High-resolution photoacoustic overtone spectrum of acetylene near 570 nm using a ring-dye-laser spectrometer. Chem Phys Lett 1991;180:310–16. doi:10.1016/0009-2614(91)90325-4.

[118] Siltanen M, Metsälä M, Vainio M, Halonen L. Experimental observation and analysis of the $3\nu_1$ stretching vibrational state of acetylene using continuous-wave infrared stimulated emission. J Chem Phys 2013;139:054201. doi:10.1063/1.4816524.

[119] Scherer GJ, Lehmann KK, Klemperer W. The high resolution visible overtone spectrum of acetylene. J Chem Phys 1983;78:2817–32. doi:10.1063/1.445269.

[120] Lyulin OM, Campargue A, Mondelain D, Kassi S. The absorption spectrum of acetylene by CRDS between 7244 and 7918 cm^{-1}. J Quant Spectrosc Radiat Transf 2013;130:327–34. doi:10.1016/j.jqsrt.2013.04.028.

[121] Lyulin OM, Mondelain D, Beguier S, Kassi S, Auwera JV, Campargue A. High-sensitivity CRDS absorption spectroscopy of acetylene between 5851 and 6341 cm^{-1}. Mol Phys 2014;112:2433–44. doi:10.1080/00268976.2014.906677.

[122] Kassi S, Lyulin OM, Béguier S, Campargue A. New assignments and a rare peculiarity in the high sensitivity CRDS spectrum of acetylene near 8000 cm^{-1}. J Mol Spectrosc 2016;326:106–14. doi:10.1016/j.jms.2016.02.013.

[123] Rothman LR, Jacquemart D, Barbe A, Benner DC, Birk M, Brown LR, et al. The HITRAN 2004 molecular spectroscopic database. J Quant Spectrosc Radiat Transf 2005;96:139–204. doi:10.1016/j.jqsrt.2004.10.008.

[124] Rothman LS, Gordon IE, Barbe A, Benner DC, Bernath PF, Birk M, et al. The HITRAN 2008 molecular spectroscopic database. J Quant Spectrosc Radiat Transf 2009;110:553–72.

[125] Rothman LS, Gordon IE, Babikov Y, Barbe A, Benner DC, Bernath PF, et al. The HITRAN 2012 molecular spectroscopic database. J Quant Spectrosc Radiat Transf 2013;130:4–50. doi:10.1016/jqsrt.2013.07.002.

[126] Chubb K.L., Yurchenko S.N., Yachmenev A., Tennyson J.. TROVE: treating linear molecule HCCH. J Chem Phys, (to be submitted).

[127] Sousa-Silva C., McKemmish L.K., Chubb K.L., Baker J., Barton E., Gorman M.N., et al. Original research by young twinkle students (ORBYTS): when can students start performing original research. Phys Educ. (submitted).